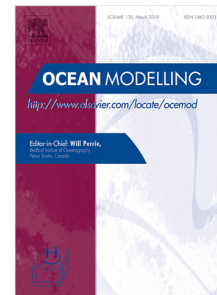


Journal Pre-proof

The impact of ocean biogeochemistry on physics and its consequences for modelling shelf seas

Jozef Skákala, Jorn Bruggeman, David Ford, Sarah Wakelin,
Anıl Akpınar, Tom Hull, Jan Kaiser, Benjamin R. Loveday,
Enda O’Dea, Charlotte A.J. Williams, Stefano Ciavatta



PII: S1463-5003(22)00026-9
DOI: <https://doi.org/10.1016/j.ocemod.2022.101976>
Reference: OCEMOD 101976

To appear in: *Ocean Modelling*

Received date: 12 April 2021
Revised date: 22 December 2021
Accepted date: 4 February 2022

Please cite this article as: J. Skákala, J. Bruggeman, D. Ford et al., The impact of ocean biogeochemistry on physics and its consequences for modelling shelf seas. *Ocean Modelling* (2022), doi: <https://doi.org/10.1016/j.ocemod.2022.101976>.

This is a PDF file of an article that has undergone enhancements after acceptance, such as the addition of a cover page and metadata, and formatting for readability, but it is not yet the definitive version of record. This version will undergo additional copyediting, typesetting and review before it is published in its final form, but we are providing this version to give early visibility of the article. Please note that, during the production process, errors may be discovered which could affect the content, and all legal disclaimers that apply to the journal pertain.

© 2022 Published by Elsevier Ltd.

1 Highlights

2 **The impact of ocean biogeochemistry on physics and its conse-**
3 **quences for modelling shelf seas**

4 Jozef Skákala, Jorn Bruggeman, David Ford, Sarah Wakelin, Anıl Akpınar,
5 Tom Hull, Jan Kaiser, Benjamin R. Loveday, Enda O’Dea, Charlotte A.J.
6 Williams, Stefano Ciavatta

- 7 • We show that, within the shelf sea environment, biogeochemistry has
8 an important impact on sea temperature and vertical mixing.
- 9 • We demonstrate that the simulated physics is quite sensitive to the
10 adopted light scheme within the physical-biogeochemical model.
- 11 • We improved the representation of the biogeochemical feedback to
12 physics in the research version of the operational model for the North-
13 West European Shelf and we have shown that this development im-
14 proves the timing of the phytoplankton bloom.
- 15 • We have validated the performance of the newly updated model within
16 the context of assimilative experiments used in the standard operational
17 set-up.

18 The impact of ocean biogeochemistry on physics and its
 19 consequences for modelling shelf seas

20 Jozef Skákala^{a,b}, Jorn Bruggeman^a, David Ford^c, Sarah Wakelin^d, Anıl
 21 Akpınar^d, Tom Hull^{e,f}, Jan Kaiser^f, Benjamin R. Loveday^g, Enda O’Dea^c,
 22 Charlotte A.J. Williams^d, Stefano Ciavatta^{a,b}

^a*Plymouth Marine Laboratory, Prospect Place, The Hoe, Plymouth, PL1 3DH, United Kingdom*

^b*National Centre for Earth Observation, Prospect Place, The Hoe, Plymouth, PL1 3DH, United Kingdom*

^c*Met Office, FitzRoy Road, Exeter, EX1 3PB, United Kingdom*

^d*National Oceanography Centre, Joseph Proudman Building, 6 Brownlow Street, Liverpool, L3 5DA, United Kingdom*

^e*Centre for Environment, Fisheries and Aquaculture Science, Lowestoft, NR33 0HT, United Kingdom*

^f*Centre for Ocean and Atmospheric Science, University of East Anglia, Norwich, NR4 7TJ, United Kingdom*

^g*Innoflair UG, Richard-Wagner-Weg 35, Darmstadt, 64287, Germany*

23 **Abstract**

We use modelling and assimilation tools to explore the impact of biogeochemistry on physics in the shelf sea environment, using North-West European Shelf (NWES) as a case study. We demonstrate that such impact is significant: the attenuation of light by biogeochemical substances heats up the upper 20 m of the ocean by up to 1°C and by a similar margin cools down the ocean within the 20-200 m range of depths. We demonstrate that these changes to sea temperature influence mixing in the upper ocean and feed back into marine biology by influencing the timing of the phytoplankton bloom, as suggested by the critical turbulence hypothesis. We compare different light schemes representing the impact of biogeochemistry on physics, and show that the physics is sensitive to both the spectral resolution of radiances and the represented optically active constituents. We introduce a new development into the research version of the operational model for the NWES, in which we calculate the heat fluxes based on the spectrally resolved attenuation by the simulated biogeochemical tracers, establishing a two-way coupling between biogeochemistry and physics. We demonstrate that in the

late spring-summer the two-way coupled model increases heating in the upper oceanic layer compared to the existing model and improves by 1-3 days the timing of the simulated phytoplankton bloom. This improvement is relatively small compared with the existing model bias in bloom timing, but is sufficient to have a visible impact on model skill in the free run. We also validate the skill of the two-way coupling in the context of the weakly coupled physical-biogeochemical assimilation currently used for operational forecasting of the NWES. We show that the change to the skill is negligible for analyses, but it remains to be seen how much it differs for the forecasts.

24 *Keywords:* impact of biogeochemistry on physics, two-way coupled
 25 physical-biogeochemical model, ocean chlorophyll concentration, sea surface
 26 temperature, phytoplankton spring bloom, North-West European Shelf
 27 (10E-10W, 40N-68N), data assimilation, operational systems

28 1. Introduction

29 Within the Earth system, physics and biology mutually interact in many
 30 non-trivial ways. In the marine environment biological processes are driven
 31 by physical transport, mixing, temperature, salinity and the incoming light,
 32 whereas biology impacts physics through its role in the carbon cycle (mi-
 33 crobial and biological pump, e.g [1]), oceanic albedo ([2]), underwater light
 34 attenuation ([3, 4, 5, 6, 7, 8, 9, 10, 11, 12, 13, 14]), and its influence on
 35 cloud condensation nuclei through the production of dimethyl sulfide (DMS,
 36 [15, 16, 17, 18]), or through bubble formation ([19]). While the impact of
 37 physics on biology is never neglected or disputed, the impact of biology on
 38 physics became often a matter of controversy, for example in connection with
 39 “the Gaia hypothesis” ([20, 21]), which proposes that life plays a central role
 40 in regulating climate. Marine model development largely reflects this under-
 41 lying scientific attitude, i.e. the common way to simplify complex coupled
 42 physical-biogeochemical dynamics is to neglect the impact of the simulated
 43 biogeochemistry on physics ([22, 23, 24]), so that the physical component can
 44 be run entirely independently of the biogeochemical model (we will further
 45 call such models “one-way coupled”).

46 The most obvious source of biogeochemical feedback to physics in coupled
 47 physical-biogeochemical ocean models is the attenuation of underwater radi-
 48 ances by optically active biogeochemical tracers and the subsequent impact
 49 on heat fluxes, temperature and mixed layer depth (MLD). One-way coupled

50 models either do not represent this effect at all, or they incorporate it “offline”
51 based on external forcing, such as using observational products for surface
52 diffuse attenuation coefficients (e.g. [25]). However, since our overall goal
53 is to realistically represent environmental processes, or to produce reliable
54 global climate projections, it is a matter of importance to better understand
55 both the biogeochemical impact on ocean physics, and the sensitivity of the
56 simulated physics to how precisely such an impact is incorporated into the
57 physical model. Only by answering these two questions can we see to what
58 extent the simplifications usually adopted in our models are justified.

59 Studies have looked at the impact of biogeochemical light attenuation on
60 marine physics, e.g in the North Atlantic ([7]), tropical Pacific ([11]) and glob-
61 ally ([8]), demonstrating that the impact can be substantial, but regionally-
62 dependent. However, the studies so far largely focused on the open ocean
63 that dominates the global scales, and there is a lack of a more detailed study
64 of such impact in the shelf sea environment. Shelf seas are highly produc-
65 tive parts of the ocean ([26, 27]), which makes them particularly relevant to
66 study the complex interaction between biogeochemistry and physics. In this
67 study we will employ state-of-the-art modelling tools (e.g. [28]) to estimate
68 the impact of biogeochemical tracers on vertical light and heat attenuation
69 on the North-West European Shelf (NWES), a region of particular interest
70 for the European economy ([29]) and carbon cycle ([26, 27]). Furthermore,
71 we will determine how sensitive the physical model of the NWES is to the
72 adopted light scheme used to drive the heat fluxes in the water column.

73 As part of the work described in this study we implemented, into the
74 physical model within a research version of the Copernicus Marine Environ-
75 ment Monitoring Service (CMEMS) operational system for the NWES, a
76 state-of-the-art representation of underwater radiances. This uses the spec-
77 trally resolved bio-optical module from [28], based on the OASIM model
78 of [30]. Since the attenuation in the newly implemented module is calcu-
79 lated using the simulated biogeochemical tracers, the physics now depends
80 on the simulated biogeochemistry (henceforth, we will refer to such models
81 as “two-way coupled”, for examples see [7, 8, 11]). We will provide a detailed
82 evaluation of the updated system performance including the weakly coupled
83 physical-biogeochemical data assimilation. The aim of this evaluation is to
84 provide a recommendation of whether the new set-up should be considered
85 for operational use.

86 A specific problem of focus for this study is the impact of the changed
87 physics (within the newly introduced two-way coupled model) on the simu-

lated biogeochemistry. The existing CMEMS operational system is one-way coupled, and it has been argued ([28]) that it may be underestimating the heating in the upper ocean, at least relative to the newly introduced two-way coupled model. The expected increase in upper-ocean heating due to two-way coupling is likely to reduce convective mixing in the upper ocean ([31, 32]), which may change the timing of the spring phytoplankton bloom, as per the critical turbulence hypothesis ([33, 34]). To be more specific: although many factors can influence the bloom timing (including biological drivers, such as zooplankton grazing, e.g. [35]), the critical turbulence hypothesis is one of the leading hypotheses for how blooms are triggered in the North Atlantic, suggesting that the bloom happens when the effective mixing depth is fully contained within the lit layer. Reducing convective mixing can then reduce the effective mixing depth and trigger an earlier phytoplankton bloom (for the mechanism see the schematic in Fig.1), which would be desirable, as the current operational model is known to produce late and intense spring blooms ([28, 36]). Since a spring bloom is a major ecosystem driver on the NWES ([37, 38]), any improvements in bloom timing could have an important knock-on effect on the biogeochemical model skill.

The questions outlined in this study will be addressed by analysing outputs of a number of suitably designed free and assimilative runs. The paper will be structured as follows: Firstly we will describe the model, light scheme and, if present, the assimilation set-up for the different simulations, as well as the methodology on how to validate and compare those different simulations. This will be followed by the section describing the results on the sensitivity of temperature to the light attenuation by the biogeochemical tracers, as well as to the adopted light scheme, and also on the impact of two-way coupling and assimilation on the coupled physical-biogeochemical model skill. In the last part we will discuss our results and outline the directions for future research.

2. Methods

2.1. The physical model: Nucleus for European Modelling of the Ocean (NEMO)

The NEMO ocean physics component (OPA) is a finite difference, hydrostatic, primitive equation ocean general circulation model ([25]). The NEMO configuration used in this study is similar to the one used by [39, 40, 28], and identical to the configuration used in [36]: we use the CO6 NEMO version, based on NEMOv3.6, a development of the CO5 configuration explained in detail by [41]. The model has 7 km spatial resolution on the Atlantic Margin

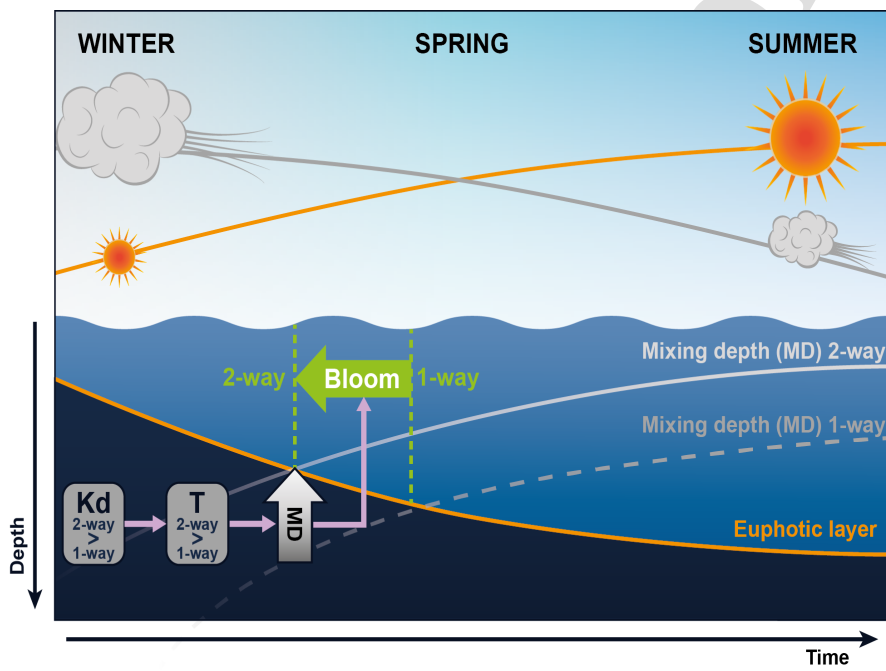


Figure 1: A schematic representation of the hypothesis about the impact of the two-way coupled model on the timing of the simulated bloom.

124 Model (AMM7) domain using a terrain-following $z^* - \sigma$ coordinate system
125 with 51 vertical levels ([42]). The lateral boundary conditions for physical
126 variables at the Atlantic boundary were taken from the outputs of the Met
127 Office operational 1/12° North Atlantic model (NATL12, [43]); the Baltic
128 boundary values were derived from a reanalysis produced by the Danish Me-
129 teorological Institute for CMEMS. We used river discharge based on data
130 from [44]. The model was forced at the surface by atmospheric fluxes pro-
131 vided by an hourly and 31 km resolution realisation (HRES) of the ERA5
132 data-set (<https://www.ecmwf.int/>).

133 This paper compares several light schemes previously used in the litera-
134 ture to calculate the NEMO oceanic heat fluxes (for the summary see Tab.1):

135 (i) The existing reanalysis version of the operational one-way coupled
136 model (e.g. [40]), which takes the total incoming net shortwave radiation
137 from the ERA5 data, splits it into visible (400-700 nm) and invisible fraction,
138 with the visible fraction attenuated inside the water column based on the K_d
139 for 490 nm wavelength supplied by a monthly climatology from an Ocean
140 Color - Climate Change Initiative (OC-CCI) product of European Space
141 Agency (ESA), version 4.1 (<https://www.esa-oceancolour-cci.org/>), and the
142 invisible waveband attenuated with a constant e-folding depth of 0.35 m.

143 (ii) The red-green-blue (RGB) scheme by [11], which uses the visible frac-
144 tion of light spectrally resolved into 3 wavebands: blue (400-500 nm), green
145 (500-600 nm) and red (600-700 nm) and attenuates it by the sea water and
146 phytoplankton chlorophyll. By default, chlorophyll is taken to be a constant
147 0.05 mg/m^3 , a minimal value representative of oligotrophic waters, as in
148 [11, 41, 45]. Alternatively, chlorophyll can be simulated by a biogeochemical
149 model, as in [11]. Both these chlorophyll schemes will be included into our
150 study.

151 (iii) The two-way coupled run using the implementation of a bio-optical
152 module based on the OASIM model ([46, 47, 28]), providing spectrally (in 33
153 wavebands) resolved radiance decomposed into direct and diffuse streams.
154 For a detailed description of the bio-optical module and the attenuation
155 scheme see the next section describing the European Regional Seas Ecosystem
156 Model (ERSEM) model.

157 (iv) We will also use the scheme based on the bio-optical module to sim-
158 ulate the attenuation by clear water-only, to provide a baseline run for the
159 comparison of how biology and the different light schemes impact physics on
160 the NWES.

161 In each of the previous cases, the underwater radiances are at every ver-

162 tical level integrated by NEMO to calculate the heating within each vertical
163 layer as

$$\frac{dT}{dt} = \frac{dI}{dz} \cdot \frac{1}{C\rho}, \quad (1)$$

164 where T is temperature, t is time, dI is, for each vertical model layer, the
165 difference between the irradiance penetrating the top of a grid box and that
166 leaving the bottom, dz is the vertical distance between the top and bottom
167 of the grid box, C is heat capacity and ρ is the reference water density.

Table 1: The different light schemes forcing the heat fluxes in the physical NEMO model. The abbreviations can be explained as follows: chlorophyll a : “Chl a ”, “ady”: ERSEM tracer representing absorption by particulate organic matter (POM), colored dissolved organic matter (CDOM) and sediment.

abbreviation	two-way coupling	source of incoming SWR	resolved	attenuation scheme	the studies using this scheme
NO-BGC	no	bio-optical module	33 bands, diffuse, direct	OASIM only clear water	—
1-WAY	no	ERA5	visible, invisible (2 bands)	visible: 490nm K_d product, invisible: clear water	[40, 28, 36]
1-WAY-RGB-CC	no	ERA5	visible: 3-bands (RGB), invisible: 1-band	visible: 0.05mg/m ³ Chl a , visible, invisible: clear water	[11, 41, 45]
2-WAY-RGB-SC	yes	ERA5	visible: 3-bands (RGB), invisible: 1-band	visible: ERSEM Chl a , visible, invisible: clear water	[11]
2-WAY	yes	bio-optical module	33 bands, diffuse, direct	OASIM, ERSEM 4 PFT Chl a , forced ady, clear water	—

168 2.2. The ecosystem model: the European Regional Seas Ecosystem Model 169 (ERSEM)

170 ERSEM ([48, 49, 50]) is a lower trophic level ecosystem model for ma-
171 rine biogeochemistry, pelagic plankton, and benthic fauna ([51]). In this
172 study, ERSEM is coupled to the physical model NEMO using Framework
173 for Aquatic Biogeochemical Models (FABM, [52, 53]). ERSEM splits phy-
174 toplankton into four functional types largely based on their size ([48]): pi-
175 cophytoplankton, nanophytoplankton, diatoms and dinoflagellates. ERSEM
176 uses variable stoichiometry for the simulated plankton groups ([54, 55]) and
177 each Phytoplankton Functional Type (PFT) biomass is represented in terms

178 of chlorophyll, carbon, nitrogen and phosphorus, with diatoms also repre-
179 sented by silicon. ERSEM predators are composed of three zooplankton
180 types (mesozooplankton, microzooplankton and heterotrophic nanoflagel-
181 lates), with organic material being decomposed by one functional type of
182 heterotrophic bacteria ([49]). The ERSEM inorganic component consists of
183 nutrients (nitrate, phosphate, silicate, ammonium and carbon) and dissolved
184 oxygen. The carbonate system is also included in the model ([56]).

185 We applied in this study the ERSEM configuration from [36], based on a
186 new ERSEM version 20.10, which has an updated benthic component with
187 respect to [49]. The ERSEM parametrization is identical to the one described
188 in [49]. The Atlantic boundary values for nitrate, phosphate, silicate and
189 oxygen were taken from World Ocean Atlas ([57]) and dissolved inorganic
190 carbon from the GLODAP gridded dataset ([58, 59]), while plankton and
191 detritus variables were set to have zero fluxes at the Atlantic boundary.

192 The irradiance at the ocean surface was calculated for all the runs us-
193 ing the bio-optical module implemented into the NEMO-FABM-ERSEM
194 AMM7 configuration by [28]. The bio-optical module resolves irradiance
195 spectrally (33 wavebands in the 250-3700 nm range) and distinguishes be-
196 tween downwelling direct and diffuse streams. The module is forced by the
197 ERA5 atmospheric inputs (<https://www.ecmwf.int/>) for total vertically in-
198 tegrated ozone, water vapour, cloud cover, cloud liquid water and sea-level
199 air pressure, as well as by a satellite product for aerosol optical thickness
200 (MODerate resolution Imaging Spectroradiometer, MODIS, [https://modis-
201 gsfc.nasa.gov/data/dataproduct](https://modis.gsfc.nasa.gov/data/dataproduct)), and also by data for surface wind speed, air
202 humidity, and air temperature, all provided by the NEMO atmospheric
203 (ERA5) forcing. The attenuation of the irradiance was described in detail
204 by [47, 28], here it is briefly summarized: The module distinguishes between
205 the absorption and scattering by the sea water and the 4 PFTs, based on the
206 wavelength-dependent absorption, total scattering and backscattering coef-
207 ficients from [47]. Although we included the impact of backscattering on
208 the light attenuation, similarly to [28], we argue that explicitly tracking the
209 upwelling stream can be reasonably neglected. Besides the clear sea water
210 and PFTs, we included into the light attenuation also the absorption by
211 POM, CDOM and sediment, which was (the same as in [28]) forced by an
212 external product extrapolated from the 443 nm data of [60]. The bio-optical
213 module was extensively validated in [28], and was shown to be skilled in its
214 representation of SWR, PAR and the underwater irradiances.

215 Finally, all the ERSEM simulations in this study used the bio-optical

216 module described in the previous paragraph, but in the case of the NO-BGC
 217 run (for abbreviations see Tab.1) all the attenuation except by the clear sea
 218 water was removed. The choice of ERSEM light scheme for the different
 219 simulations is justified as follows:

220 a) The 1-WAY and 2-WAY configurations using the bio-optical module
 221 to force ERSEM, correspond to the latest research version of the CMEMS
 222 system on the NWES (the 1-WAY configuration, see [28]) and the currently
 223 most advanced version of the coupled NEMO-FABM-ERSEM model on the
 224 NWES (the 2-WAY configuration).

225 b) To sensibly compare the impact of biogeochemistry on physics it is im-
 226 portant that the 2-WAY-RGB-SC run (Tab.1) uses the same ERSEM light
 227 module as the 2-WAY run. This ensures that the simulated biogeochemical
 228 tracers are between the different two-way coupled runs consistent to a max-
 229 imum possible degree, in the sense that the only differences in the ERSEM
 230 tracers are caused by the differences in the NEMO physics (transport, mix-
 231 ing, temperature), triggered by the different NEMO light schemes.

232 c) In case of both, NO-BGC and 1-WAY-RGB-CC runs, NEMO is entirely
 233 independent from ERSEM. It is also expected that the physics in the NO-
 234 BGC and 1-WAY-RGB-CC will be the most different from the remaining
 235 three free simulations. To estimate the size of the impact of the NEMO
 236 simulated physical state on the ERSEM simulated biogeochemistry, relative
 237 to the size of the impact of the radiances seen by ERSEM, whilst minimising
 238 the number of necessary simulations included in the study, we decided to
 239 use the same ERSEM light scheme for the 1-WAY-RGB-CC run as for the
 240 1-WAY, 2-WAY and 2-WAY-RGB-SC runs, but using the same light scheme
 241 for ERSEM as in NEMO for the NO-BGC run.

242 *2.3. The assimilative system: NEMOVAR*

243 NEMOVAR is a variational (in this study a 3DVar) DA system ([61, 62,
 244 63]) used at the Met Office for operational forecasting and reanalyses on
 245 the NWE Shelf. The assimilation of ocean color-derived chlorophyll using
 246 NEMOVAR is highly successful in improving the NWE Shelf phytoplankton
 247 phenology, PFT community structure (using PFT chlorophyll assimilation),
 248 underwater irradiance and to a more limited degree also carbon cycle ([40, 28,
 249 64]). NEMOVAR includes capability to assimilate multi-platform (satellite,
 250 in situ) data, which has been established first for physics (e.g. [63, 65])
 251 and subsequently for biogeochemistry ([66]), including validating the multi-
 252 platform DA system for the NWES ([36]).

253 The NEMOVAR set-up used in this study for the multi-platform physical-
 254 biogeochemical assimilation is the same as the one described in detail by [36].
 255 Here we offer only a short summary: The 3DVar version of NEMOVAR uses
 256 a First Guess at Appropriate Time (FGAT) to calculate a daily set of in-
 257 crements for the directly updated variables ([63, 65]). In the physical DA
 258 application, NEMOVAR applies balancing relationships within the assimila-
 259 tion step and delivers a set of increments for temperature, salinity, sea surface
 260 height (SSH) and the horizontal velocity components. For the total chloro-
 261 phyll assimilation NEMOVAR calculates a set of log-chlorophyll increments
 262 and then a balancing scheme is used to distribute those increments into the
 263 PFT components (chlorophyll, carbon, nitrogen, phosphorus and for diatoms
 264 also silicon), all of which are updated based on the background community
 265 structure and stoichiometric ratios (e.g. [40, 28, 36]). After the assimilation
 266 step, the model is re-run with the increments applied to the model variables
 267 gradually at each model time-step using incremental analysis updates (IAU,
 268 [67]).

269 NEMOVAR uses externally supplied spatio-temporally varying observa-
 270 tion and background error variances, with the background error variances
 271 typically 1-3 times larger than the observational error variances ([36]). The
 272 system combines two horizontal correlation length-scales, one fixed at 100 km
 273 and the other based on the baroclinic Rossby radius of deformation ([65]).
 274 The vertical length-scales follow the scheme from [65], where NEMOVAR
 275 calculates directly the set of 3D increments using flow-dependent vertical
 276 length-scales (ℓ), which are at the surface equal to half of the MLD, decreas-
 277 ing in the mixed layer to become two-times the vertical model grid spacing
 278 at, and beneath the MLD.

279 *2.4. Observations: assimilated and validation data*

280 *2.4.1. Assimilated data*

281 In the physical data assimilation component we have included:

282 a) sea surface temperature data from the GCOM-W1/AMSR-2, NOAA/AVHRR,
 283 MetOp/AVHRR, MSG/SEVIRI, Sentinel-3/SLSTR, Suomi-NPP/VIIRS satel-
 284 lite products and in situ SST observations from ships, surface drifters and
 285 moorings, distributed over the Global Telecommunication System (GTS) in
 286 near-real time,

287 b) temperature and salinity from the EN4 dataset ([68]), which includes
 288 in situ profiles from Argo floats, fixed moored arrays, XBTs, CTDs, gliders,
 289 marine mammals, and

290 c) temperature and salinity data from a specific Slocum glider Cabot
 291 (Unit 345, see [36]) that was deployed in the central North Sea during
 292 08/05/2018 - 15/08/2018 as a part of the Alternative Framework to As-
 293 sess Marine Ecosystem Functioning in Shelf Seas (AlterECO) programme
 294 (<https://altereco.ac.uk/>). The satellite SST was bias-corrected following the
 295 scheme from [69], using the VIIRS and in situ SST data as the reference.

296 In the biogeochemical data assimilation we have included total log-chlorophyll
 297 derived from the version 4.2 of the European Space Agency (ESA) ocean-
 298 colour (OC) Climate Change Initiative (CCI) product ([70]) and also log-
 299 chlorophyll derived from the quenching corrected fluorescence measurements
 300 by the same AlterEco glider Cabot, that was used in the physical data as-
 301 similation. The assimilation is performed for log-chlorophyll, rather than
 302 chlorophyll, as chlorophyll is widely known to be log-normally distributed
 303 ([71]).

304 The assimilated in situ (EN4 and glider) observations were thinned to a
 305 resolution of 0.08° (EN4), or up-scaled to the AMM7 grid (glider), with addi-
 306 tional temporal averaging applied to the same-day glider observations. The
 307 thinning/up-scaling is performed to avoid assimilating many observations
 308 at higher resolution than the model can represent. After the thinning/up-
 309 scaling there were $O(10^5)$ EN4 and $O(10^4)$ Cabot glider data-points to as-
 310 simulate throughout the year 2018.

311 *2.4.2. Validation data*

312 The assimilated data, mentioned in the previous section, were also used
 313 to validate every experiment where they were excluded from the assimilation
 314 (e.g. assimilated chlorophyll data were used to validate free runs and the
 315 physical data assimilative runs). However, we excluded the bias-corrected
 316 satellite SST from the temperature validation, so that the only assimilated
 317 SST data used for validation were a) the high quality SST data from the
 318 VIIRS satellite product and from ships, drifters and moorings (we will call
 319 this “VIIRS/in situ SST data”), and the SST that was part of b) EN4 and
 320 c) Cabot glider data.

321 Besides the assimilated observations, all the experiments were validated
 322 with other (non-assimilated) AlterEco glider data for temperature, salinity,
 323 chlorophyll, oxygen and the sum of nitrate and nitrite (all the gliders in-
 324 cluded in the validation are listed in Tab.2). The processing of the physical,
 325 chlorophyll and oxygen data was described in [36]. The sum of nitrate and
 326 nitrite concentrations (abbreviated as $\text{NO}_x^- = \text{NO}_3^- + \text{NO}_2^-$) were determined

327 using a Lab-on-Chip (LoC) analyser designed and fabricated at the National
328 Oceanography Centre ([72]), which was implemented by the AlterEco team
329 into Seagliders following a similar protocol as used by [73]. The combined un-
330 certainty (random and systematic errors) of measurements made using these
331 LoC analysers has been calculated as $<5\%$ (coverage interval $k = 1$) ([74]).
332 The nitrite concentrations were relatively negligible compared to the nitrate
333 concentrations, so the NO_x^- data were used to validate model nitrate outputs.
334 All the data used here is from AlterEco gliders that were in operation in the
335 central North Sea during 2018 (for both the glider and the EN4 data loca-
336 tions see Fig.S1 of the Supporting Information (SI)), moving throughout the
337 whole water column. Similar to the assimilated Cabot glider, the remaining
338 glider data were up-scaled onto the model grid (on a daily basis) and after
339 the up-scaling there remained $O(10^4)$ AlterEco glider observations for each
340 variable in 2018.

341 The EN4 data-set contained subsurface observations that were approx-
342 imately homogeneously distributed both with depth and in time, with a
343 slightly lower number of observations towards the end of the year (November-
344 December 2018). Beyond the assimilated data and the AlterEco data, we
345 used for validation a 1960-2014 monthly climatological dataset for total
346 chlorophyll, oxygen, nitrate, phosphate and silicate concentrations, compiled
347 during the North Sea Biogeochemical Climatology (NSBC) project ([75]).
348 The NSBC dataset covers most of the NWE Shelf and the full range of
349 depths. Finally, we also included validation of surface CO_2 fugacity using
350 2018 SOCAT (v2019) data (<https://www.socat.info/index.php/about/>).

351 *2.5. The experiments*

352 As outlined in Tab.1 we have run multiple free simulations including both
353 one-way coupled and two-way coupled runs. We also tested the impact of
354 assimilating different types of data (physical-only, biogeochemical-only and
355 physical and biogeochemical jointly, see Tab.3) on the skill of both 1-WAY
356 and the 2-WAY models. The various free and assimilative experiments used
357 exactly the same model configuration, apart from the differences outlined in
358 Tab.1 and Tab.3. The experiments all started from the same initial value
359 conditions on the 01/09/2017 to allow a 4 month spin-up time for the final
360 2018 simulation. The initial values were provided by the 2016-2018 free
361 simulation (using bio-optical module) from the study of [28].

Table 2: The AlterEco gliders and the variables measured by the gliders used for assimilation (6-th column), or validation (7-th column). The table uses the following abbreviations: deployment:“dpl”, data assimilation:“DA”, temperature:“T”, salinity:“S”, oxygen concentrations:“O₂”, chlorophyll *a* concentrations:“Chl *a*” and sum of nitrate and nitrite concentrations:“NO_x⁻”.

Campaign	platform	dpl	serial	mission period	DA	validation
AlterEco 1	Stella	440	unit_436	02/02/2018 - 08/05/2018	none	T,S,O ₂ ,Chl <i>a</i>
AlterEco 1	Cook	441	unit_194	15/11/2017 - 07/02/2018	none	T,S,O ₂ ,Chl <i>a</i> ,NO _x ⁻
AlterEco 2	Orca	493	SG510	07/03/2018 - 27/03/2018	none	Chl <i>a</i> ,NO _x ⁻
AlterEco 2	Melonhead	496	SG620	07/02/2018 - 02/04/2018	none	Chl <i>a</i>
AlterEco 3	Cabot	454	unit_345	08/05/2018 - 15/08/2018	T,S,Chl <i>a</i>	T,S,O ₂ ,Chl <i>a</i>
AlterEco 3	Orca	455	SG510	16/03/2018 - 24/07/2018	none	Chl <i>a</i> ,NO _x ⁻
AlterEco 3	Humpback	497	SG579	09/05/2018 - 25/06/2018	none	Chl <i>a</i>
AlterEco 4	Dolomite	477	unit_305	13/08/2018 - 10/10/2018	none	T,S,Chl <i>a</i> ,NO _x ⁻
AlterEco 4	Eltanin	478	SG550	15/08/2018 - 28/09/2018	none	Chl <i>a</i>
Altereco 5	Kelvin	481	unit_444	26/09/2018 - 02/12/2018	none	T,S,Chl <i>a</i>
AlterEco 6	Dolomite	499	unit_305	02/12/2018 - 12/03/2018	none	T,S,O ₂ ,Chl <i>a</i>
AlterEco 6	Coprolite	500	unit_331	02/12/2018 - 12/03/2018	none	T,S,O ₂ ,Chl <i>a</i>

Table 3: The different assimilative experiments compared in this study. The first column shows the abbreviated experiment name, where the last word in the name (“1-WAY”, “2-WAY”) refers to the baseline model configuration (see the third and sixth row of Tab.1) and the following columns list the assimilated data. The table uses the following abbreviations: satellite:“sat”, Cabot glider:“Cabot”, EN4 dataset:“EN4”, temperature:“T”, sea surface temperature:“SST”, salinity:“S”, chlorophyll *a*:“Chl *a*”.

abbreviation	SST (sat./in situ)	T & S (EN4)	T & S (Cabot)	Chl <i>a</i> (sat.)	Chl <i>a</i> (Cabot)
PHYS DA 1-WAY	yes	yes	yes	no	no
PHYS DA 2-WAY	yes	yes	yes	no	no
CHL DA 1-WAY	no	no	no	yes	yes
CHL DA 2-WAY	no	no	no	yes	yes
PHYS+CHL DA 1-WAY	yes	yes	yes	yes	yes
PHYS+CHL DA 2-WAY	yes	yes	yes	yes	yes

362 *2.6. Skill metrics*

363 The performance of the different simulations is evaluated using two skill
364 metrics. The first metric is the model bias (ΔQ_{mo}):

$$\Delta Q_{mo} = \langle Q_m - Q_o \rangle \quad (2)$$

365 where Q_o are the observations mapped into the model grid and the Q_m are
366 the corresponding model outputs. The second metric is the bias-corrected
367 root mean square difference (BC RMSD, $\Delta_{RD}Q_{mo}$):

$$\Delta_{RD}Q_{mo} = \sqrt{\langle (Q_m - Q_o - \Delta Q_{mo})^2 \rangle}. \quad (3)$$

368 **3. Results**

369 *3.1. The impact of biogeochemistry on physics on the NWES*

370 To determine the overall impact of biogeochemical light attenuation on
371 the NWES temperature vertical profiles, we compare the simulation based
372 on the bio-optical module using only clear water attenuation (NO-BGC)
373 with the two-way coupled run using the bio-optical module and assimilating
374 chlorophyll into the model (CHL DA 2-WAY). The CHL DA 2-WAY run
375 is chosen because it provides us with the best representation of the biogeo-
376 chemical feedback to physics including the most realistic simulation of the
377 phytoplankton distributions.

378 Fig.2 shows that NWES biogeochemistry has a substantial impact on the
379 simulated temperature in the late spring-summer, heating up the upper 20
380 m in the water column and cooling down the water column beneath the
381 mixed layer, almost down to the 200 m depth. The temperature variations
382 due to biogeochemistry are, in the warmest summer period, on the scale of
383 $\pm 1^\circ\text{C}$. The geographical impact of biogeochemistry on temperature (Fig.3:A)
384 is largest in the northern part of the North Sea. Conversely, it is by far the
385 lowest in the English Channel and the southern part of the North Sea. The
386 heating of the uppermost ocean layer has an important impact (up to 20%)
387 on the mixing depth, which is consistently shallowed by the biogeochemistry
388 across the whole NWES (Fig.3:C).

389 All the results presented in this section are broadly consistent with the
390 findings of [8] for the global domain and [7] more specifically for the North
391 Atlantic domain.

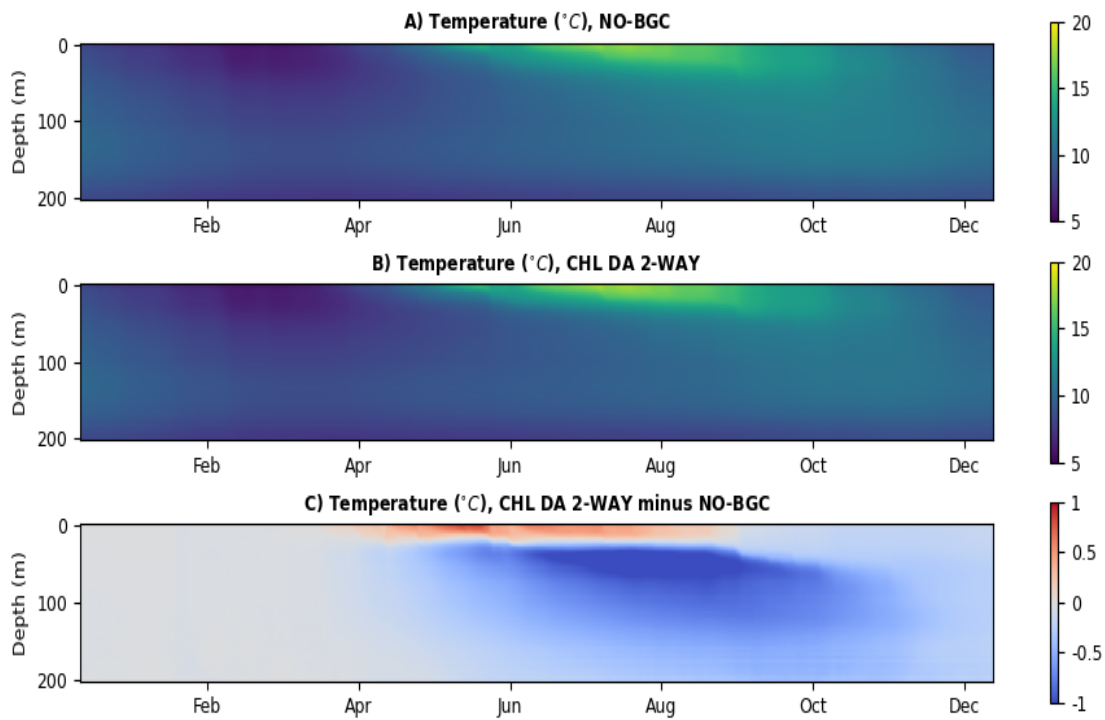


Figure 2: Panel A shows a Hovmöller diagram (depth on the y-axis vs time on the x-axis) for the temperature (°C) of the run with only sea water attenuation. The values for each day and depth represent the horizontal spatial averages throughout the NWES (bathymetry < 200 m, see the boundary in Fig.3). Panel B shows the same Hovmöller diagram as panel A, but for the CHL DA 2-WAY run (for the abbreviations used in the titles see Tab.3), whereas panel C shows the difference between the two runs shown in the panels A and B (panel B minus panel A).

Proof

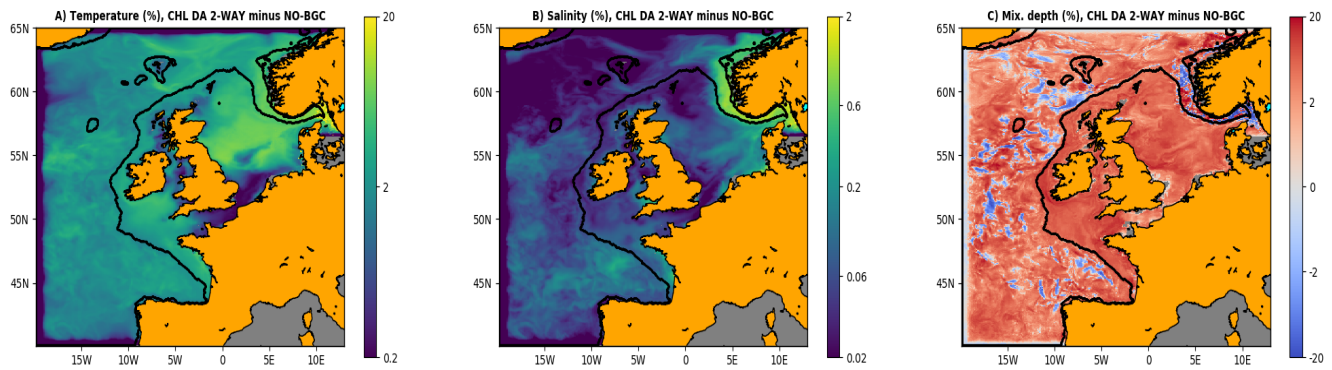


Figure 3: The spatial regions of biogeochemical impact on temperature (A, in %), salinity (B, in %) and mixing depth (C, in %). For temperature and salinity the panels show 2018 and vertically (up to 200 m depth) averaged absolute difference between the CHL DA 2-WAY and NO-BGC runs normalized by the values of the NO-BGC run (in case of temperature, the normalization is relative to Celsius). For mixing depth (defined as the maximum depth of the column where the temperature difference between top and bottom layer is less than 0.2°C) we show the mean 2018 difference between CHL DA 2-WAY and NO-BGC runs normalized by the NO-BGC run. The boundary of the NWES (bathymetry < 200m) is marked by the black line.

392 *3.2. Comparing the impact of different light schemes on physics*

393 We compare the sensitivity of simulated temperature and MLD to the
 394 light schemes, incorporating the impact of biogeochemistry on the light at-
 395 tenuation seen by the NEMO physical model (Tab.1). Fig.4 and Fig.5 com-
 396 pare the temperature of all the simulations using different light schemes to
 397 the NO-BGC run. Fig.4 shows that the two-way coupled model based on the
 398 bio-optical module (2-WAY, panel D) produces an increase of near-surface
 399 attenuation, and hence sea temperature, when compared to the one-way cou-
 400 pled run forced by an external satellite product (1-WAY, panel B, for direct
 401 comparison between the two runs see also Fig.S2 of the Supporting Informa-
 402 tion, SI).

403 Since the physical model skill depends on many components within the
 404 complex model, there can be many error compensations ([28]). It is, there-
 405 fore, hard to validate the performance of the NEMO light scheme indepen-
 406 dently of the specific context in which it was implemented. However, Fig.5
 407 should still give an indication of how the different light schemes compare with
 408 the 3D glider observations along the glider trajectory. Fig.5 illustrates that
 409 neglecting the biogeochemical impact on light attenuation in the NO-BGC
 410 run produces a spurious heating effect of up to 3°C beneath the upper 30 m
 411 in the water column. Including biogeochemical impact on the temperature
 412 reduces this model bias to below 1°C (Fig.5:B-E).

413 *3.3. The sensitivity of biogeochemistry to the changes in underwater radiance
 414 and mixing*

415 ERSEM is known to simulate a late phytoplankton spring bloom on the
 416 NWES (e.g. Fig.6 and Fig.7). As suggested by the critical turbulence hy-
 417 pothesis, the bloom timing depends on both, the light seen by the phyto-
 418 plankton, and vertical mixing (e.g. Fig.1). The ERSEM sensitivity to light
 419 is demonstrated by the NO-BGC simulation. Due to absence of biogeochem-
 420 ical impact on the underwater radiances in the NO-BGC run, there is an
 421 excess of light deep within the water column and this provides (despite the
 422 deep winter mixing) good phytoplankton growth conditions over the winter,
 423 with an early bloom triggered around late February (Fig.6:B). The only se-
 424 riously limiting factor to the surface chlorophyll abundance in the NO-BGC
 425 run seem to be nutrients in the post-bloom period (Fig.6:B).

426 In the remaining free run simulations, ERSEM always uses the same light
 427 scheme, but the physical NEMO model does not. The different light schemes
 428 in the physical model produce different vertical mixing and slightly modify

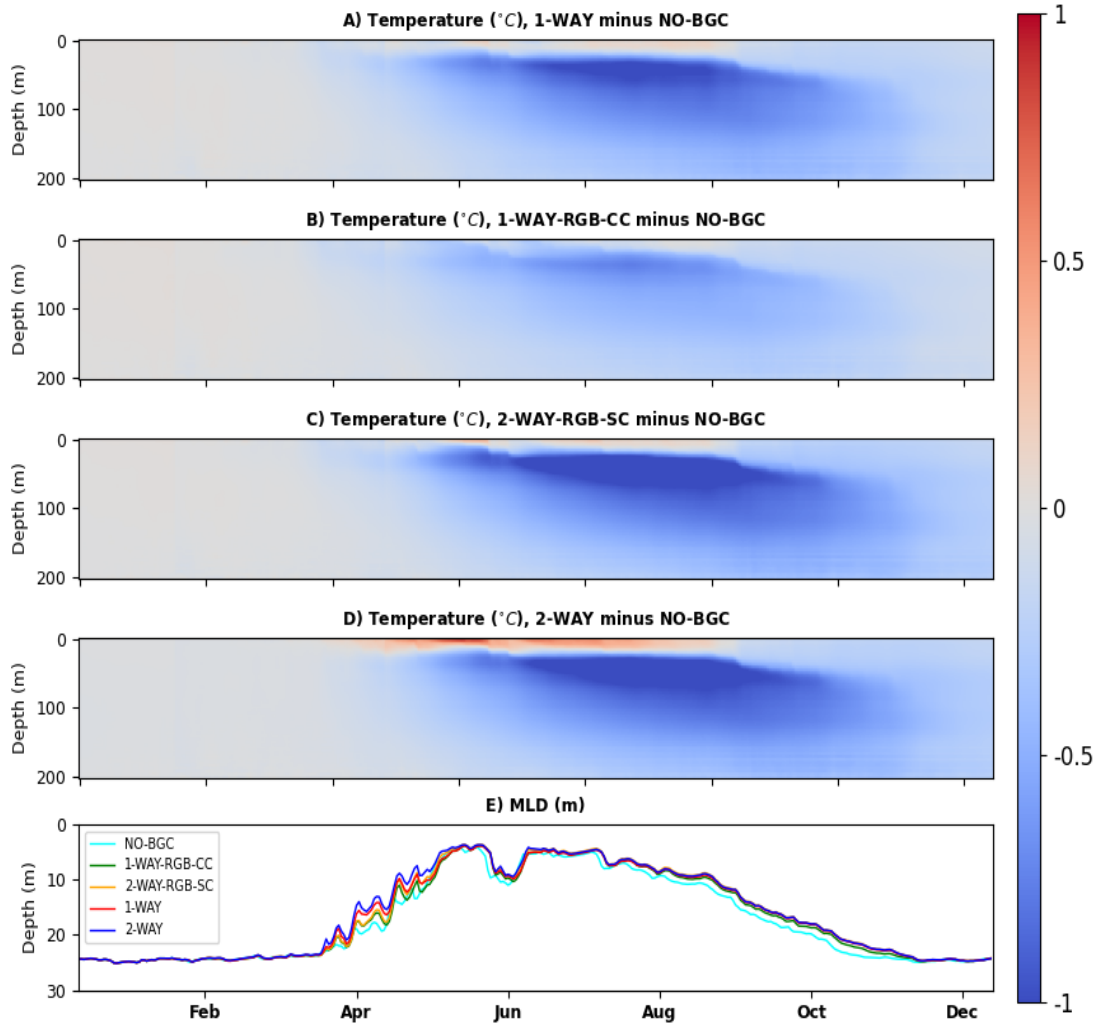


Figure 4: Panels A-D are similar to Fig.2:C and show Hovmöller diagrams for the horizontally averaged differences in temperature (in $^{\circ}\text{C}$, averaged across NWES) between the different light schemes and the NO-BGC run. Panel E compares the 2018 time series for MLD (in m) horizontally averaged across the NWES.

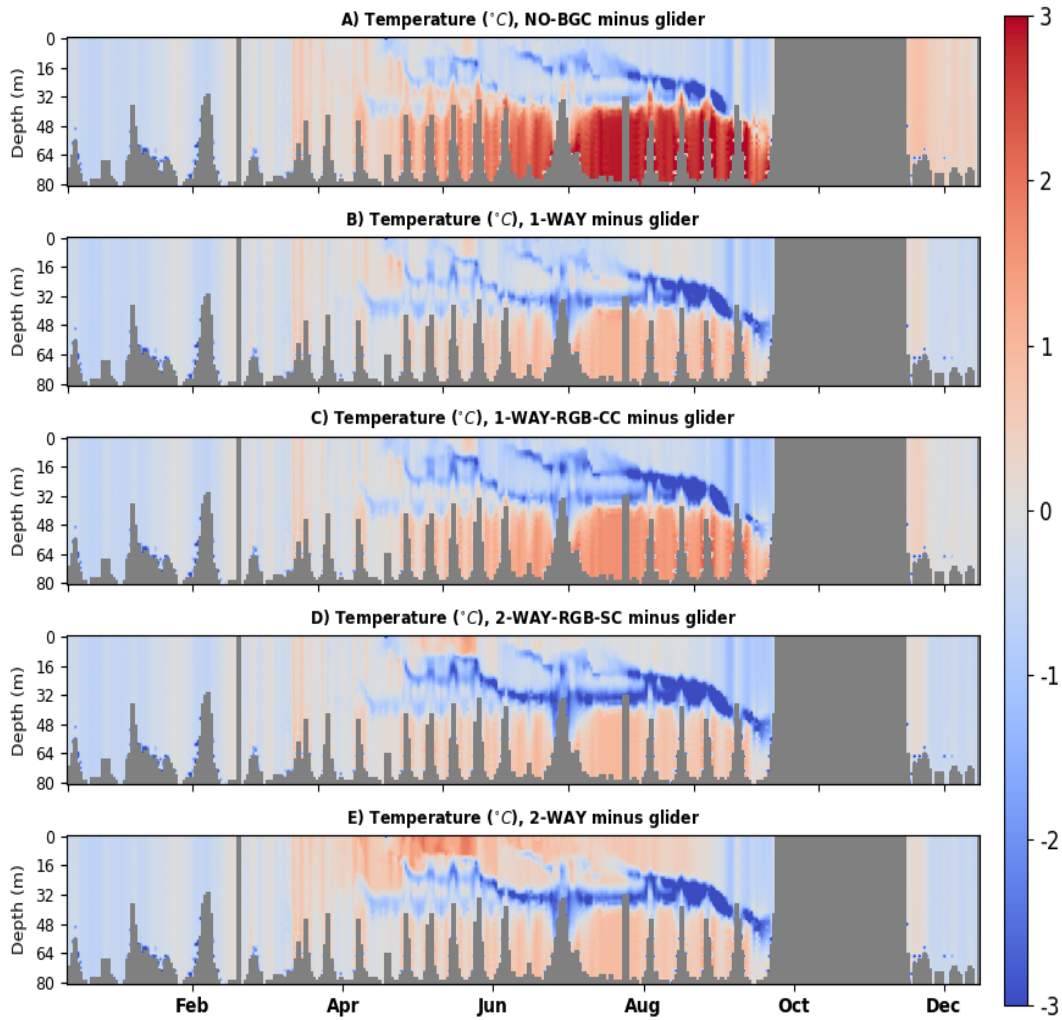


Figure 5: Hovmöller diagrams comparing the temperature (in °C) in the different free runs to the glider data along the glider trajectory.

429 the timing of the phytoplankton bloom (Fig.6:C-D). For example, the in-
430 creased near-surface absorption in the 2-WAY model increases heating in the
431 upper oceanic layer with respect to the 1-WAY run (Fig.4:B,D), reduces con-
432 vective mixing, and for most of the NWES, moves the model bloom towards
433 the start of the year by 1-3 days, but in some specific locations (e.g. in the
434 central North Sea) the bloom can be as much as 5 days earlier in the 2-WAY
435 run than in the 1-WAY run (Fig.6:C,E, Fig.7:C, Fig.8).

436 *3.4. The potential impact of two-way coupling on the skill of the CMEMS* 437 *operational system*

438 Introducing two-way coupling into the CMEMS operational model would
439 correspond to a transition from the 1-WAY to the 2-WAY model set-up,
440 but also include the assimilation of physical and biogeochemical data. As
441 previously discussed in the free run, the transition from 1-WAY to 2-WAY
442 run produces extra heating in the upper 20 m of the ocean, increasing sea
443 temperature by around 1°C, and by a similar margin cooling down the 20-100
444 m layer beneath the surface (compare Fig4:A and Fig.4:D, Fig.S2:B of the
445 SI). This marginally shallows the MLD (Fig.4:E).

446 In the summer (May-October), when the impact of two-way coupling is
447 largest, the 2-WAY run reduces the temperature bias of the 1-WAY run,
448 however it increases the SST bias and BC RMSD (Fig.9:A). In the winter
449 (November-April), the impact of two-way coupling on the model tempera-
450 ture is also mixed (Fig.9:B), as it is for salinity throughout the whole year
451 (Fig.9:C-D). The changes to physics introduced by the 2-WAY set-up (rela-
452 tive to 1-WAY) have a positive impact on the timing of the phytoplankton
453 bloom (Fig.6:C,E, Fig.7:C), which leads to improvement in model skill in
454 representing phytoplankton chlorophyll *a* (Fig.10:A). Interestingly, correct-
455 ing phytoplankton phenology through the OC chlorophyll assimilation has
456 also a positive impact on the simulated temperature and salinity in the 2-
457 WAY run (Fig.9). Fig.9 also demonstrates that the physical (temperature
458 and salinity) assimilation substantially improves model skill in representing
459 both temperature (Fig.9:A-B) and salinity (Fig.9:C-D). The physical data as-
460 similation influences the simulated temperature more evenly across the water
461 column than the bio-optical module (Fig.S2 of SI), which is likely a combi-
462 nation of model dynamical response to the temperature increments in the
463 mixed layer and some assimilated sub-surface data (EN4 and Cabot glider).

464 The chlorophyll assimilation improves the simulated chlorophyll (Fig.10:A),
465 and dominates over both physical assimilation and two-way coupling in its

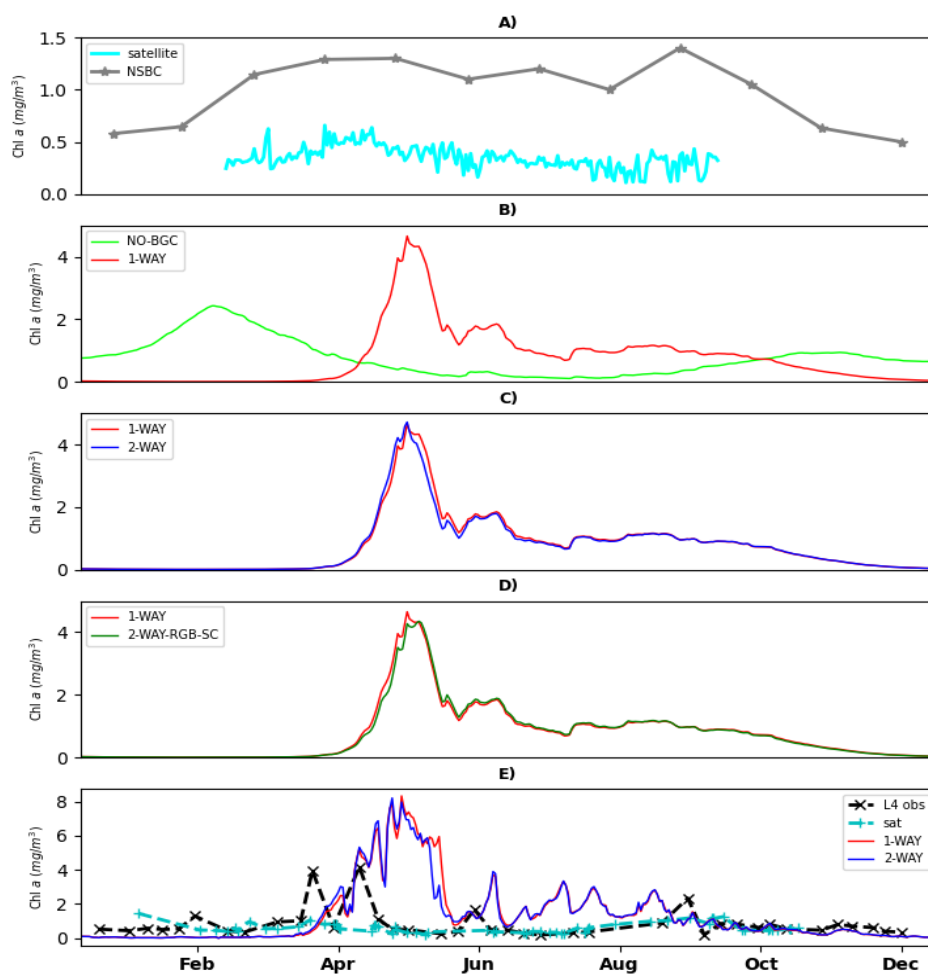


Figure 6: Panels A-D show the 2018 time-series for the surface chlorophyll (mg/m^3) averaged across the NWES. Panel A is showing the satellite OC observations and NSBC climatology, whilst panels B-D compare the selected light schemes. The last panel E compares the model, satellite and in situ observations at the L4 station in the English Channel.

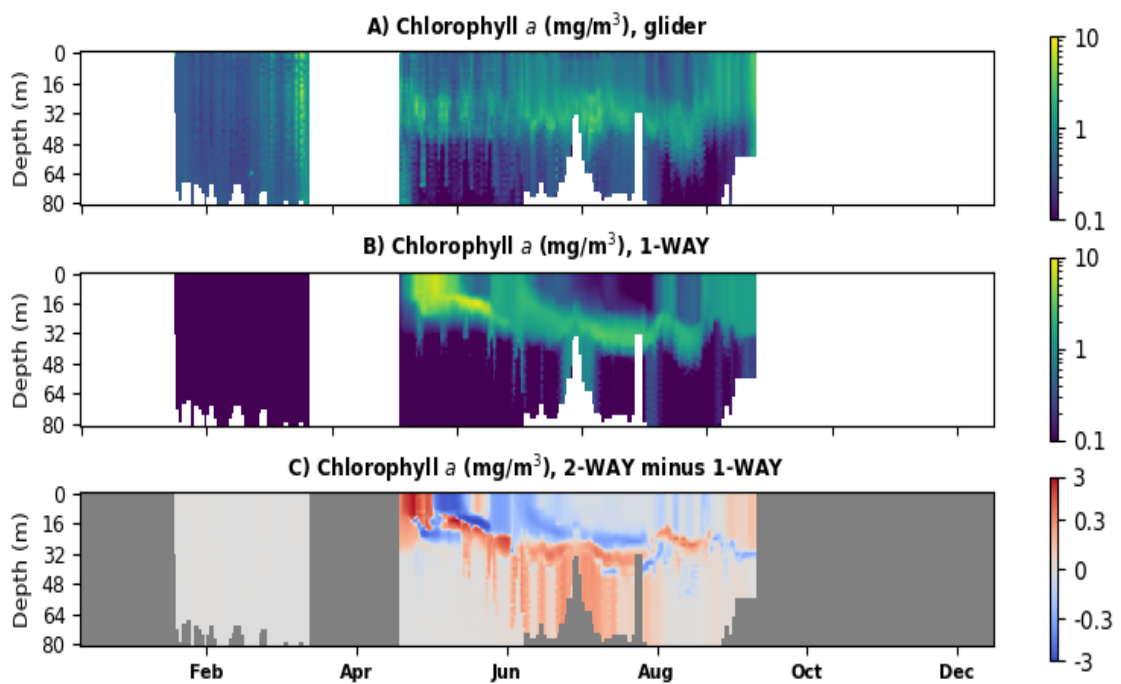


Figure 7: Panels A-B show Hovmöller diagrams for chlorophyll (mg/m^3) observed by the AlterEco gliders (A) and simulated in the 1-WAY run across the glider trajectory (B). Panel C compares the 2-WAY and 1-WAY runs across the glider trajectory.

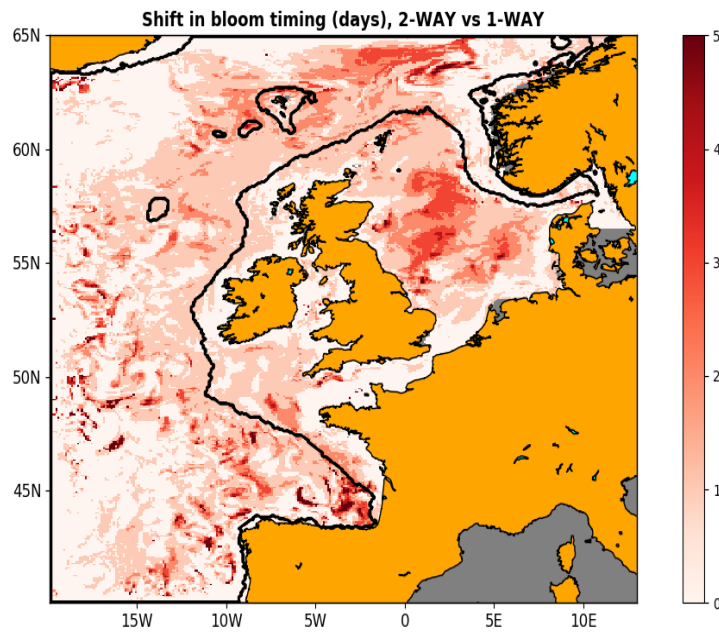


Figure 8: The spatial distribution for the time-lag (in days) between the earlier bloom of the 2-WAY run and the later bloom of the 1-WAY run. The time-shift in the bloom was calculated by taking for each location the April-June total chlorophyll *a* time-series from both 1-WAY, 2-WAY, runs, extracting only the data when at least one of the runs had chlorophyll concentrations over 2 mg/m^3 threshold, and calculating from those data the time-lag with the highest lagged Pearson correlation between the two time-series.

466 impact on the simulated chlorophyll concentrations across the whole water
467 column over the whole simulation year (Fig.S3 of SI). That this would be the
468 case is not obvious, as the chlorophyll assimilation is almost entirely based on
469 the satellite OC and chlorophyll beneath the mixed layer is updated mostly
470 through the model dynamical adjustment. The bloom dynamics is also cor-
471 rected by the chlorophyll assimilation (Fig.S4 of SI), which is consistent with
472 the previous studies ([28, 36]).

473 To get a more complete view of the impact of two-way coupling on the
474 simulated biogeochemistry, we also looked at the available data for oxygen,
475 CO₂ fugacity, nitrate, phosphate and silicate. Fig.10 shows that the two-way
476 coupling may also improve the modelled oxygen (Fig.10:B) and CO₂ fugacity
477 (Fig.10:C), which is, in both cases, a combined result of changes to air-sea
478 fluxes (due to changes in sea temperature and therefore gas saturation levels),
479 to the primary productivity (change to bloom timing) and consequently also
480 changes to respiration levels. Physical and chlorophyll *a* assimilation tend to
481 have additional positive impact on oxygen and CO₂ fugacity (Fig.10:B-C).
482 The impact of the two-way coupled model on nutrients is mostly driven by
483 the changes to primary productivity and phytoplankton, and is shown to be
484 fairly negligible (Fig.10:C-F). These results are broadly consistent with the
485 previous literature ([40, 28]), which showed that chlorophyll *a* assimilation
486 can have an important impact on the nutrient concentrations, but often has
487 a mixed effect in terms of the model skill to represent nutrients (Fig.10).

488 4. Discussion

489 On the NWES, there is a strong seasonal dependence of the biogeochem-
490 ical impact on temperature (Fig.2) which can be easily understood: in the
491 late autumn to early spring period the water column is very well mixed and
492 this averages out the vertical changes to heating caused by the presence of
493 biogeochemical tracers. In the late spring, when the water column becomes
494 much more stratified, the biogeochemical substances trap light and heat in
495 the uppermost layer, gradually cooling down the ocean beneath the upper
496 ~ 20 m. However, due to oceanic inertia, the impact of extra near-surface
497 heating introduced by the biogeochemical substances propagates only slowly
498 downwards, producing an increasingly delayed response (approximately on a
499 monthly scale) as one looks deeper into the water column (Fig.2:C). Similarly
500 to the winter period, the lack of biogeochemical impact on physics around

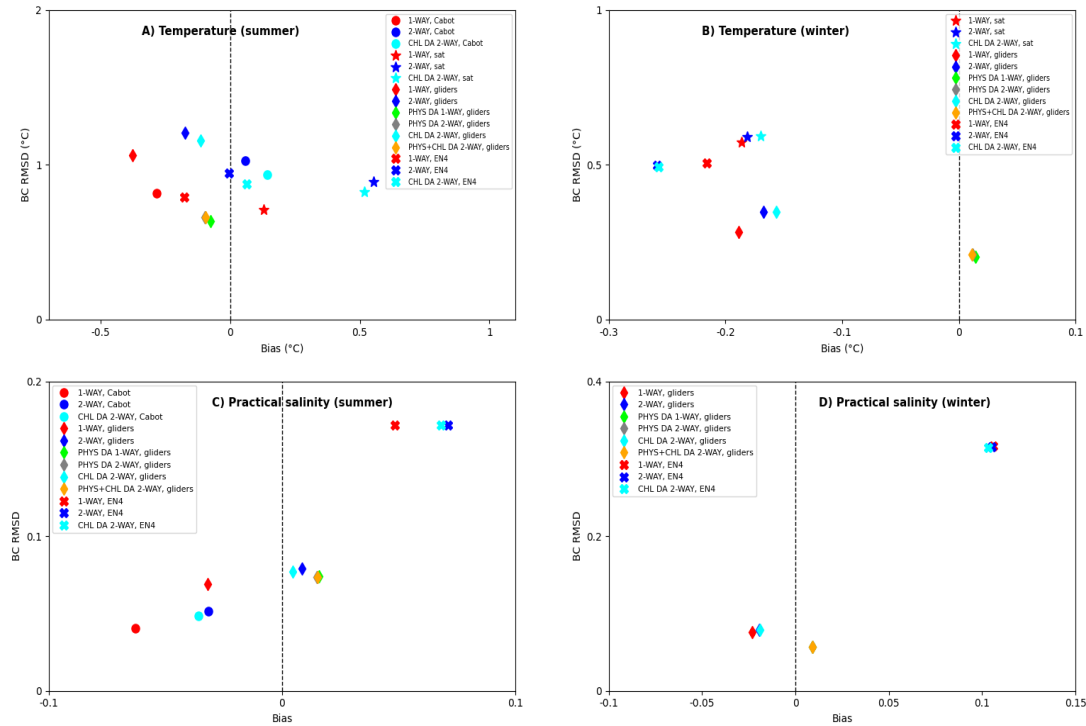


Figure 9: Skill of the different model simulations to represent temperature ($^{\circ}\text{C}$, panels A-B) and practical salinity (panels C-D). The skill is measured by bias (x-axis, Eq.2) and BC RMSD (y-axis, Eq.3). The skill is evaluated for two half-year periods of 2018, the “summer” (panels A,C) defined as May-October and the “winter” (panels B,D) defined as November-April (data averaged through January-April 2018 and November-December 2018). The different simulations are represented by different colors: 1-WAY (red), 2-WAY (blue), CHL DA 2-WAY (cyan), PHYS DA 1-WAY (lime), PHYS DA 2-WAY (grey) and PHYS+CHL DA 2-WAY (orange). The different markers show comparison with different data-sets: the star stands for the VIIRS/in situ SST, the circle for the Cabot glider observations, the diamond for the remaining available glider observations (the 2018 AlterEco mission without Cabot) and the cross for the EN4 data-set. The data (SST, Cabot, EN4) which were assimilated in some of the simulations were used to validate only the simulations that avoided their assimilation.

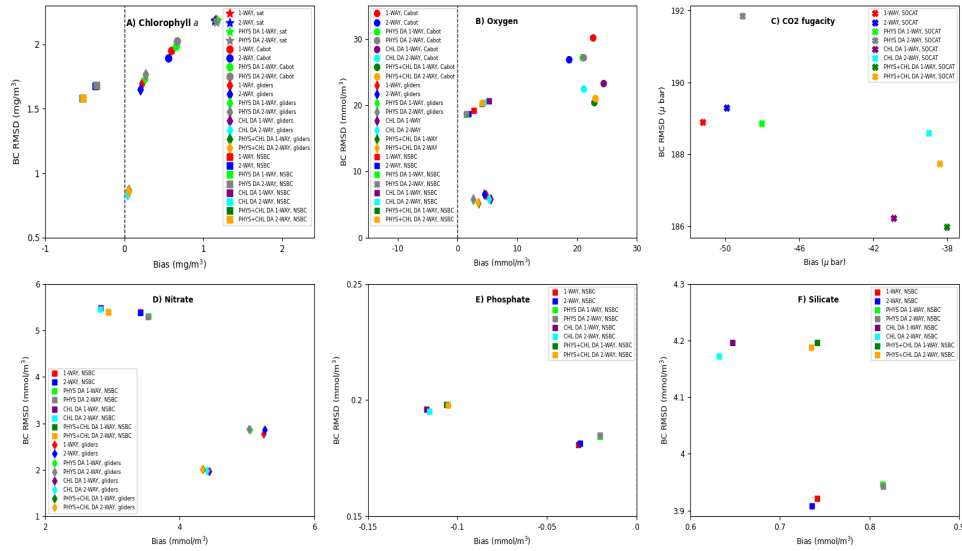


Figure 10: Skill of the different model simulations to represent chlorophyll *a* (mg/m³, panel A), oxygen (mmol/m³, panel B), CO₂ fugacity (μ bar, panel C), nitrate (mmol/m³, panel D), phosphate (mmol/m³, panel E) and silicate (mmol/m³, panel F) concentrations. The skill is measured by bias (x-axis, Eq.2) and BC RMSD (y-axis, Eq.3). The skill is evaluated for the full year 2018. The different simulations are represented by different colors: 1-WAY (red), 2-WAY (blue), CHL DA 1-WAY (purple), CHL DA 2-WAY (cyan), PHYS DA 1-WAY (lime), PHYS DA 2-WAY (grey), PHYS+CHL DA 1-WAY (green) and PHYS+CHL DA 2-WAY (orange). The different markers show comparison with different data-sets: the star stands for the satellite ocean color data, the circle for the Cabot glider observations, the diamond for the remaining available glider observations (the 2018 AlterEco mission without Cabot), the cross for the SOCAT data and the square for the NSBC climatological data-set.

501 the English Channel (Fig.3) can be explained by the high levels of vertical
502 mixing in this area (see [76]).

503 The 2-WAY run produces large extra heating in the uppermost layer also
504 relative to the 1-WAY run (Fig.4:A,D). Although, in theory, the bio-optical
505 module used to drive biogeochemistry produces different incoming radiation
506 than the ERA5 forcing data used to force physics in the 1-WAY run, it has
507 been shown that there is a negligible mutual bias between the module and
508 ERA5 ([28]). Therefore, the temperature increase is likely a consequence of
509 an increased rate of absorption inside the upper oceanic layer, rather than
510 resulting from an enhanced shortwave radiation flux into the water column.
511 The increased absorption in the 2-WAY run was anticipated since: a) in a
512 previous study ([28]) the bio-optical module appeared to have higher levels of
513 light attenuation near the water surface than the satellite observations used
514 to force the physics in the one-way coupled run, b) the “broadband” visible
515 light attenuation in the 1-WAY run was represented by the satellite K_d for
516 490 nm wavelength, but K_d at 490 nm wavelength is clearly an underestimate
517 of the K_d for the 400-700 nm waveband (see Fig.5:B of [28]).

518 We can also understand the gradually increasing impact of biogeochem-
519 istry on temperature between the 1-WAY-RGB-CC, 2-WAY-RGB-SC and
520 2-WAY runs (Fig.4:B-D). The RGB scheme using constant chlorophyll (1-
521 WAY-RGB-CC, Fig.4:B, used in [11, 41, 45]) to represent oligotrophic open
522 ocean waters, clearly underestimates the overall chlorophyll concentrations
523 in the shelf seas and leads to unrealistically small attenuation of underwa-
524 ter radiance. The attenuation is increased by the more realistic simulated
525 chlorophyll in the 2-WAY-RGB-SC run (Fig.4:C), but it remains weak when
526 compared to the 2-WAY scheme, since 2-WAY-RGB-SC neglects the impact
527 of POM, CDOM and sediment on the light attenuation. These non-living
528 optically active constituents can be potentially neglected in the open ocean
529 (e.g [11]), but become more relevant in the coastal and shelf sea waters, as
530 these results demonstrate. The 2-WAY scheme (Fig.4:D) incorporates the
531 impact of all phytoplankton, POM, CDOM and sediment on the underwater
532 radiance, and therefore demonstrates the greatest impact of biogeochemistry
533 on temperature. The sensitivity of physics to biogeochemical attenuation
534 scheme, that we observed here, is also broadly consistent with an older mod-
535 elling study of [77], focusing on the seas near the south-eastern coast of Aus-
536 tralia, which has found that the simulated temperature vertical profiles and
537 some ocean circulation patterns were significantly impacted by the chloro-
538 phyll vertical attenuation scheme.

539 The shift in the bloom timing shown in Fig.8 nicely matches with the
540 regions where there is the largest biogeochemical impact on temperature
541 (Fig.3:A). This indicates that, although the bloom timing was shown not to
542 be very sensitive to the changes in convective mixing (e.g Fig.6), the small
543 changes to the bloom timing can be understood from the critical turbulence
544 hypothesis (as outlined in Fig.1). In reality the late bloom could be explained
545 by multiple components within the physical-biogeochemical coupled model,
546 such as atmospheric wind stress forcing, NEMO upper-ocean mixing scheme,
547 vertical stratification (thermocline and pycnocline), incoming surface PAR,
548 underwater light attenuation, the phytoplankton growth response to light
549 (e.g. ERSEM parameters, such as P-I curves, or maximum PFT chlorophyll-
550 to-carbon ratios), ERSEM representation of top-down grazing, or missing
551 processes such as mixotrophy (e.g. [78]). From the variety of drivers that
552 could contribute to the bloom timing, only a small fraction was so far ad-
553 dressed, i.e. [28] have showed that the late bloom is most likely not related
554 to a problem with the underwater radiances, whilst in this study we similarly
555 addressed the vertical stratification. Diagnosing the true cause of the late
556 phytoplankton bloom thus remains a challenge for the future.

557 Although the (modest) improvements to the simulated chlorophyll by the
558 2-WAY model originate from its changes to the simulated physics (i.e. ver-
559 tical mixing), it might seem surprising that the physical data assimilation,
560 which substantially improves the simulated physics (Fig.9), does not improve
561 (and even slightly degrades) the model skill in chlorophyll (Fig.10:A). This is
562 likely because the physical data assimilation is, for the large part, an assimi-
563 lation of SST. The improvement in the ecosystem model skill depends mostly
564 on the vertical mixing and limited changes to vertical mixing are expected by
565 assimilating SST. Assimilated subsurface temperature and salinity data are
566 quite sparse, and have only a limited impact on the modelled biogeochem-
567 istry. In the case of the Cabot glider “case-study”, the glider temperature
568 and salinity assimilation did not improve the simulated chlorophyll at the
569 glider locations (Fig.10:A) mostly because the impact of physics on biogeo-
570 chemistry needs some spin-up time. In fact in the last part of the glider
571 mission period (late July-August) the physical assimilation has some poten-
572 tial to improve the chlorophyll concentrations, as was demonstrated by the
573 assimilation of the same Cabot glider data in Fig.6E of [36].

574 There is only negligible difference in the skill between the PHYS+CHL
575 DA 1-WAY and PHYS+CHL DA 2-WAY runs (Fig.9 and Fig.10). This sug-
576 gests that physical and chlorophyll assimilation dominates over the two-way

577 coupling and hence, for an operational system that includes assimilation of
578 both physics and biogeochemistry, the transition to two-way coupling may
579 produce only marginal difference in the system skill. Such difference might
580 certainly be more significant for system forecasts than for the analyses (fore-
581 casting was not explored in this study). However, on the 1-day time scale the
582 forecast differences were captured by the difference in innovations (defined
583 as background minus observations) and this was found to be negligible, e.g.
584 the 2018 and spatial mean difference in the SST innovations between the
585 PHYS+CHL DA 1-WAY and PHYS+CHL DA 2-WAY runs was found to be
586 less than 0.01°C .

587 5. Summary

588 In this work we used a recent implementation of an (OASIM-based) spec-
589 trally resolved bio-optical module into a physical-biogeochemical model of the
590 North-West European Shelf (NWES, [28]) and expanded it to drive also the
591 oceanic heat fluxes, introducing a feedback from the biogeochemical model to
592 the physics (we call the models with such feedback “two-way coupled mod-
593 els”). We used this development to estimate the scale of the biogeochemical
594 impact on physics on the NWES and we have shown that during late spring
595 and summer, when the water column is stratified, biogeochemical tracers can
596 heat up the upper 20 m of the water column by 1°C and cool down the ocean
597 beneath the upper 20 m by a similar margin. The seasonal impact of biogeo-
598 chemistry on physics propagates deeper into the water column with oceanic
599 inertia and is visible down to 200 m depth. Impact of biogeochemistry on
600 heating of the uppermost oceanic layer influences ocean vertical mixing and
601 shallows the mixing depth across the NWES by up to 20%. These results
602 suggest that it is important to represent the coupling from biogeochemistry
603 to physics adequately in our models.

604 We have looked at different light schemes used in the literature (e.g.
605 [11, 41, 45, 40]) that incorporate biogeochemical impact on light attenuation,
606 either within a two-way coupled model, or as an external parametrization,
607 or forcing (e.g. using 490 nm K_d satellite product). We have shown that the
608 simulated physics is reasonably sensitive to the different light schemes, i.e.
609 both to spectral resolution and the number of represented bio-optical tracers.

610 In the last part of this study we discussed the likely impact of introduc-
611 ing two-way coupling into the present operational CMEMS system for the
612 NWES. We have shown that the newly developed two-way coupled model,

613 based on the spectrally resolved bio-optical module, increases the heat cap-
614 tured in the upper part of the water column relative to the existing sys-
615 tem, which represents the underwater attenuation by an external 490 nm K_d
616 satellite product. The two-way coupling steepens the vertical temperature
617 gradient, shallows the mixed layer depth and reduces convective mixing. The
618 reduced vertical mixing has a modest, but positive, impact on the timing of
619 the late bloom displayed by the biogeochemical model (in line with the critical
620 turbulence hypothesis). The shift in the timing of the bloom in the two-way
621 coupled model improves the model skill in representing chlorophyll. We con-
622 clude that, for a more substantial improvement of the timing of the bloom,
623 it will be necessary to either improve the physical model mixing scheme, or
624 to improve the process description, or parametrization, of the biogeochemi-
625 cal model. We have expanded our analysis to include other biogeochemical
626 tracers, and found that the two-way coupled model and the physical data as-
627 simulation may sometimes help improve the agreement of simulated oxygen
628 concentrations and CO_2 fugacity with observations, both due to improved
629 simulation of the sea water temperature (saturation levels) and productivity.

630 Although the two-way coupled model performs slightly better than the
631 existing one-way coupled model, it was found that the difference between
632 those two becomes negligible whenever we include assimilation of physical
633 data and chlorophyll. In the future it would be desirable to explore how
634 much the impact of the two-way coupling increases during the 6-day oper-
635 ational forecasting period. Moreover, physical-biogeochemical assimilative
636 runs on the NWES, including this work, are typically only weakly coupled
637 (for one recent exception see [79]), in the sense that the physical and the bio-
638 geochemical variables are updated independently and interact only through
639 the model dynamics. The interaction between physics and biogeochemistry
640 would be much more efficient if the assimilative updates to the physics and
641 biogeochemistry interacted directly through their cross-covariances, or a bal-
642 ancing component within the data assimilation system. Such scheme is called
643 “strongly coupled”, and would provide the physical assimilation with both
644 faster and greater impact on the biogeochemical model skill, and vice versa.
645 Future work will use the improved physical-biogeochemical coupling in the
646 two-way coupled model to inform the development of the data assimilation
647 scheme to include such strong coupling in our operational system.

648 Acknowledgments

649 This work was supported by a Natural Environment Research Council
650 (NERC) funded project of the Marine Integrated Autonomous Observing
651 Systems (MIAOS) programme: Combining Autonomous observations and
652 Models for Predicting and Understanding Shelf seas (CAMPUS). It also ben-
653 efitting from another NERC funded project Alternative Framework to Assess
654 Marine Ecosystem Functioning in Shelf Seas (AlterECO, [http://projects.noc-
655 .ac.uk/altereco/](http://projects.noc.ac.uk/altereco/)), grant no. NE/P013899/1. The work also benefited from
656 the Copernicus Marine Environment Monitoring Service (CMEMS) funded
657 projects OPTical data Modelling and Assimilation (OPTIMA) and NOWMAPS.
658 Furthermore, this work was also partially funded by the SEAMLESS project,
659 which received funding from the European Union’s Horizon 2020 research
660 and innovation programme under grant agreement No 101004032. We would
661 like to thank Dawn Ashby for drawing the schematic Fig.1. The ocean color
662 data were provided by the European Space Agency Climate Initiative “Ocean
663 Color” (<https://esa-oceancolour-cci.org/>). The glider data used in the study
664 (doi:10.5285/b57d215e-065f-7f81-e053-6c86abc01a82 and doi:10.5285/b58e83f0-
665 d8f3-4a83-e053-6c86abc0bbb5) are publicly available on [https://www.bodc.ac.uk/-
667 data/published_data_library/catalogue/](https://www.bodc.ac.uk/-
666 data/published_data_library/catalogue/). We also used L4 time series for
668 chlorophyll *a* concentrations provided by the Western Channel Observatory
669 (<https://www.westernchannelobservatory.org.uk/>). The model was forced by
670 the atmospheric ERA5 product of The European Centre for Medium-Range
671 Weather Forecasts (ECMWF, <https://www.ecmwf.int/>). The river forcing
672 data used by the model were prepared by Sonja van Leeuwen and Helen
673 Powley as part of UK Shelf Seas Biogeochemistry programme (contract no.
674 NE/K001876/1) of the NERC and the Department for Environment Food
675 and Rural Affairs (DEFRA). We acknowledge use of the MONSooN system,
676 a collaborative facility supplied under the Joint Weather and Climate Re-
677 search Programme, a strategic partnership between the Met Office and the
678 NERC. The different outputs for the free run simulations and reanalyses are
679 stored on the MONSooN storage facility MASS and can be obtained upon
request.

680 References

- 681 [1] U. Riebesell, A. Körtzinger, A. Oschlies, Sensitivities of marine carbon
682 fluxes to ocean change, *Proceedings of the National Academy of Sciences*
683 106 (49) (2009) 20602–20609.

- 684 [2] Z. Jin, T. P. Charlock, W. L. Smith Jr, K. Rutledge, A parameterization
685 of ocean surface albedo, *Geophysical research letters* 31 (22) (2004).
- 686 [3] A. Morel, Optical modeling of the upper ocean in relation to its
687 biogenous matter content (case i waters), *Journal of geophysical re-*
688 *search: oceans* 93 (C9) (1988) 10749–10768.
- 689 [4] J.-y. Simonot, E. Dollinger, H. Le Treut, Thermodynamic-biological-
690 optical coupling in the oceanic mixed layer, *Journal of Geophysical Re-*
691 *search: Oceans* 93 (C7) (1988) 8193–8202.
- 692 [5] S. Sathyendranath, A. D. Gouveia, S. R. Shetye, P. Ravindran, T. Platt,
693 Biological control of surface temperature in the arabian sea, *Nature*
694 349 (6304) (1991) 54.
- 695 [6] A. M. Edwards, D. G. Wright, T. Platt, Biological heating effect of
696 a band of phytoplankton, *Journal of Marine Systems* 49 (1-4) (2004)
697 89–103.
- 698 [7] A. Oschlies, Feedbacks of biotically induced radiative heating on upper-
699 ocean heat budget, circulation, and biological production in a coupled
700 ecosystem-circulation model, *Journal of Geophysical Research: Oceans*
701 109 (C12) (2004).
- 702 [8] M. Manizza, C. Le Quéré, A. J. Watson, E. T. Buitenhuis, Bio-optical
703 feedbacks among phytoplankton, upper ocean physics and sea-ice in a
704 global model, *Geophysical Research Letters* 32 (5) (2005).
- 705 [9] B. Marzeion, A. Timmermann, R. Murtugudde, F.-F. Jin, Biophysical
706 feedbacks in the tropical pacific, *Journal of Climate* 18 (1) (2005) 58–70.
- 707 [10] C. Sweeney, A. Gnanadesikan, S. M. Griffies, M. J. Harrison, A. J.
708 Rosati, B. L. Samuels, Impacts of shortwave penetration depth on large-
709 scale ocean circulation and heat transport, *Journal of Physical Oceanog-*
710 *raphy* 35 (6) (2005) 1103–1119.
- 711 [11] M. Lengaigne, C. Menkes, O. Aumont, T. Gorgues, L. Bopp, J.-M.
712 André, G. Madec, Influence of the oceanic biology on the tropical pacific
713 climate in a coupled general circulation model, *Climate Dynamics* 28 (5)
714 (2007) 503–516.

- 715 [12] M. Jochum, S. Yeager, K. Lindsay, K. Moore, R. Murtugudde, Quantifi-
716 cation of the feedback between phytoplankton and enso in the commu-
717 nity climate system model, *Journal of Climate* 23 (11) (2010) 2916–2925.
- 718 [13] L. Zhai, C. Tang, T. Platt, S. Sathyendranath, Ocean response to at-
719 tenuation of visible light by phytoplankton in the gulf of st. lawrence,
720 *Journal of Marine Systems* 88 (2) (2011) 285–297.
- 721 [14] A. Turner, M. Joshi, E. Robertson, S. Woolnough, The effect of arabian
722 sea optical properties on sst biases and the south asian summer monsoon
723 in a coupled gcm, *Climate dynamics* 39 (3-4) (2012) 811–826.
- 724 [15] J. E. Lovelock, R. Maggs, R. Rasmussen, Atmospheric dimethyl sulphide
725 and the natural sulphur cycle, *Nature* 237 (5356) (1972) 452–453.
- 726 [16] R. J. Charlson, J. E. Lovelock, M. O. Andreae, S. G. Warren, Oceanic
727 phytoplankton, atmospheric sulphur, cloud albedo and climate, *Nature*
728 326 (6114) (1987) 655–661.
- 729 [17] K. D. Six, S. Kloster, T. Ilyina, S. D. Archer, K. Zhang, E. Maier-
730 Reimer, Global warming amplified by reduced sulphur fluxes as a result
731 of ocean acidification, *Nature Climate Change* 3 (11) (2013) 975–978.
- 732 [18] J. Schwinger, J. Tjiputra, N. Goris, K. D. Six, A. Kirkevåg, Ø. Seland,
733 C. Heinze, T. Ilyina, Amplification of global warming through ph de-
734 pendence of dms production simulated with a fully coupled earth system
735 model, *Biogeosciences* 14 (15) (2017) 3633.
- 736 [19] T. W. Wilson, L. A. Ladino, P. A. Alpert, M. N. Breckels, I. M. Brooks,
737 J. Browse, S. M. Burrows, K. S. Carslaw, J. A. Huffman, C. Judd, et al.,
738 A marine biogenic source of atmospheric ice-nucleating particles, *Nature*
739 525 (7568) (2015) 234–238.
- 740 [20] J. Lovelock, *Gaia: A new look at life on earth*, Oxford Paperbacks, 1979.
- 741 [21] J. Lovelock, *The ages of Gaia: A biography of our living earth*, Oxford
742 University Press, USA, 2000.
- 743 [22] C. Heinze, M. Gehlen, Modeling ocean biogeochemical processes and
744 the resulting tracer distributions, in: *International Geophysics*, Vol. 103,
745 Elsevier, 2013, pp. 667–694.

- 746 [23] M. Gehlen, R. Barciela, L. Bertino, P. Brasseur, M. Butenschön, F. Chai,
747 A. Crise, Y. Drillet, D. Ford, D. Lavoie, et al., Building the capacity for
748 forecasting marine biogeochemistry and ecosystems: recent advances
749 and future developments, *Journal of Operational Oceanography* 8 (sup1)
750 (2015) s168–s187.
- 751 [24] D. Ford, S. Kay, R. McEwan, I. Totterdell, M. Gehlen, Marine biogeo-
752 chemical modelling and data assimilation for operational forecasting,
753 reanalysis, and climate research, *New Frontiers in Operational Oceanog-*
754 *raphy* (2018) 625–652.
- 755 [25] G. Madec, et al., *Nemo ocean engine* (2015).
- 756 [26] A. Borges, L.-S. Schiettecatte, G. Abril, B. Delille, F. Gazeau, Carbon
757 dioxide in european coastal waters, *Estuarine, Coastal and Shelf Science*
758 70 (3) (2006) 375–387.
- 759 [27] R. A. Jahnke, Global synthesis, in: *Carbon and nutrient fluxes in con-*
760 *tinental margins*, Springer, 2010, pp. 597–615.
- 761 [28] J. Skákala, J. Bruggeman, R. J. Brewin, D. A. Ford, S. Ciavatta, Im-
762 proved representation of underwater light field and its impact on ecosys-
763 tem dynamics: a study in the north sea, *Journal of Geophysical Re-*
764 *search: Oceans* (2020) e2020JC016122.
- 765 [29] D. Pauly, V. Christensen, S. Guénette, T. J. Pitcher, U. R. Sumaila,
766 C. J. Walters, R. Watson, D. Zeller, Towards sustainability in world
767 fisheries, *Nature* 418 (6898) (2002) 689.
- 768 [30] W. W. Gregg, N. W. Casey, Skill assessment of a spectral ocean–
769 atmosphere radiative model, *Journal of Marine Systems* 76 (1-2) (2009)
770 49–63.
- 771 [31] J. R. Taylor, R. Ferrari, Shutdown of turbulent convection as a new
772 criterion for the onset of spring phytoplankton blooms, *Limnology and*
773 *Oceanography* 56 (6) (2011) 2293–2307.
- 774 [32] T. J. Smyth, I. Allen, A. Atkinson, J. T. Bruun, R. A. Harmer, R. D.
775 Pingree, C. E. Widdicombe, P. J. Somerfield, Ocean net heat flux influ-
776 ences seasonal to interannual patterns of plankton abundance, *PloS one*
777 9 (6) (2014).

- 778 [33] J. Huisman, P. van Oostveen, F. J. Weissing, Critical depth and critical
779 turbulence: two different mechanisms for the development of phyto-
780 plankton blooms, *Limnology and oceanography* 44 (7) (1999) 1781–1787.
- 781 [34] J. J. Waniek, The role of physical forcing in initiation of spring blooms
782 in the northeast atlantic, *Journal of Marine Systems* 39 (1-2) (2003)
783 57–82.
- 784 [35] M. J. Behrenfeld, E. S. Boss, Student’s tutorial on bloom hypotheses
785 in the context of phytoplankton annual cycles, *Global change biology*
786 24 (1) (2018) 55–77.
- 787 [36] J. Skákala, D. A. Ford, J. Bruggeman, T. Hull, J. Kaiser, R. R. King,
788 B. R. Loveday, M. R. Palmer, T. J. Smyth, C. A. J. Williams, S. Ciavatta,
789 Towards a multi-platform assimilative system for ocean biogeo-
790 chemistry, *Earth and Space Science Open Archive ESSOAr*, submitted
791 to JGR-Oceans (2021).
- 792 [37] M. J. Lutz, K. Caldeira, R. B. Dunbar, M. J. Behrenfeld, Seasonal
793 rhythms of net primary production and particulate organic carbon flux
794 to depth describe the efficiency of biological pump in the global ocean,
795 *Journal of Geophysical Research: Oceans* 112 (C10) (2007).
- 796 [38] S. A. Henson, J. P. Dunne, J. L. Sarmiento, Decadal variability in
797 north atlantic phytoplankton blooms, *Journal of Geophysical Research:
798 Oceans* 114 (C4) (2009).
- 799 [39] D. A. Ford, J. van der Molen, K. Hyder, J. Bacon, R. Barciela,
800 V. Creach, R. McEwan, P. Ruardij, R. Forster, Observing and modelling
801 phytoplankton community structure in the north sea, *Biogeosciences*
802 14 (6) (2017) 1419–1444.
- 803 [40] J. Skákala, D. Ford, R. J. Brewin, R. McEwan, S. Kay, B. Taylor,
804 L. de Mora, S. Ciavatta, The assimilation of phytoplankton functional
805 types for operational forecasting in the northwest european shelf, *Jour-
806 nal of Geophysical Research: Oceans* 123 (8) (2018) 5230–5247.
- 807 [41] E. O’Dea, R. Furner, S. Wakelin, J. Siddorn, J. While, P. Sykes, R. King,
808 J. Holt, H. Hewitt, The co5 configuration of the 7 km atlantic margin
809 model: large-scale biases and sensitivity to forcing, physics options and
810 vertical resolution, *Geoscientific Model Development* 10 (8) (2017) 2947.

- 811 [42] J. Siddorn, R. Furner, An analytical stretching function that combines
812 the best attributes of geopotential and terrain-following vertical coordi-
813 nates, *Ocean Modelling* 66 (2013) 1–13.
- 814 [43] D. Storkey, E. Blockley, R. Furner, C. Guiavarc’h, D. Lea, M. Martin,
815 R. Barciela, A. Hines, P. Hyder, J. Siddorn, Forecasting the ocean state
816 using nemo: The new foam system, *Journal of operational oceanography*
817 3 (1) (2010) 3–15.
- 818 [44] H.-J. Lenhart, D. K. Mills, H. Baretta-Bekker, S. M. Van Leeuwen,
819 J. Van Der Molen, J. W. Baretta, M. Blaas, X. Desmit, W. Kühn,
820 G. Lacroix, et al., Predicting the consequences of nutrient reduction on
821 the eutrophication status of the north sea, *Journal of Marine Systems*
822 81 (1-2) (2010) 148–170.
- 823 [45] J. A. Graham, E. O’Dea, J. Holt, J. Polton, H. T. Hewitt, R. Furner,
824 K. Guihou, A. Brereton, A. Arnold, S. Wakelin, et al., Amm15: a new
825 high-resolution nemo configuration for operational simulation of the eu-
826 ropean north-west shelf, *Geoscientific Model Development* 11 (2) (2018)
827 681–696.
- 828 [46] W. W. Gregg, N. W. Casey, Modeling coccolithophores in the global
829 oceans, *Deep Sea Research Part II: Topical Studies in Oceanography*
830 54 (5-7) (2007) 447–477.
- 831 [47] W. W. Gregg, C. S. Rousseaux, Directional and spectral irradiance in
832 ocean models: effects on simulated global phytoplankton, nutrients, and
833 primary production, *Frontiers in Marine Science* 3 (2016) 240.
- 834 [48] J. Baretta, W. Ebenhöf, P. Ruardij, The european regional seas ecosys-
835 tem model, a complex marine ecosystem model, *Netherlands Journal of*
836 *Sea Research* 33 (3-4) (1995) 233–246.
- 837 [49] M. Butenschön, J. Clark, J. N. Aldridge, J. I. Allen, Y. Artioli, J. Black-
838 ford, J. Bruggeman, P. Cazenave, S. Ciavatta, S. Kay, et al., Ersem
839 15.06: a generic model for marine biogeochemistry and the ecosystem
840 dynamics of the lower trophic levels, *Geoscientific Model Development*
841 9 (4) (2016) 1293–1339.
- 842 [50] P. M. L. Marine Systems Modelling Group, European regional seas
843 ecosystem model (2020). doi:<http://doi.org/10.5281/zenodo.3817997>.

- 844 [51] J. Blackford, An analysis of benthic biological dynamics in a north sea
845 ecosystem model, *Journal of Sea Research* 38 (3-4) (1997) 213–230.
- 846 [52] J. Bruggeman, K. Bolding, A general framework for aquatic biogeochem-
847 ical models, *Environmental modelling & software* 61 (2014) 249–265.
- 848 [53] J. Bruggeman, K. Bolding, Framework for aquatic biogeochemical mod-
849 els (2020). doi:<http://doi.org/10.5281/zenodo.3817997>.
- 850 [54] R. Geider, H. MacIntyre, T. Kana, Dynamic model of phytoplankton
851 growth and acclimation: responses of the balanced growth rate and the
852 chlorophyll a: carbon ratio to light, nutrient-limitation and temperature,
853 *Marine Ecology Progress Series* 148 (1997) 187–200.
- 854 [55] J. Baretta-Bekker, J. Baretta, W. Ebenhöf, Microbial dynamics in the
855 marine ecosystem model ersem ii with decoupled carbon assimilation
856 and nutrient uptake, *Journal of Sea Research* 38 (3-4) (1997) 195–211.
- 857 [56] Y. Artioli, J. C. Blackford, M. Butenschön, J. T. Holt, S. L. Wakelin,
858 H. Thomas, A. V. Borges, J. I. Allen, The carbonate system in the north
859 sea: Sensitivity and model validation, *Journal of Marine Systems* 102
860 (2012) 1–13.
- 861 [57] H. E. Garcia, R. A. Locarnini, T. P. Boyer, J. I. Antonov, O. K. Bara-
862 nova, M. M. Zweng, J. R. Reagan, D. R. Johnson, A. V. Mishonov,
863 S. Levitus, *World ocean atlas 2013. volume 4, dissolved inorganic nutri-
864 ents (phosphate, nitrate, silicate)* (2013).
- 865 [58] R. M. Key, A. Olsen, S. van Heuven, S. K. Lauvset, A. Velo, X. Lin,
866 C. Schirnick, A. Kozyr, T. Tanhua, M. Hoppema, et al., Global ocean
867 data analysis project, version 2 (glodapv2) (2015).
- 868 [59] S. K. Lauvset, R. M. Key, A. Olsen, S. van Heuven, A. Velo, X. Lin,
869 C. Schirnick, A. Kozyr, T. Tanhua, M. Hoppema, et al., A new global
870 interior ocean mapped climatology: The 1 × 1 glodap version 2, *Earth
871 System Science Data* 8 (2016) 325–340.
- 872 [60] T. J. Smyth, Y. Artioli, Global inherent optical properties from SeaW-
873 iFS data (2010). doi:[10.1594/PANGAEA.741913](https://doi.org/10.1594/PANGAEA.741913).
874 URL <https://doi.org/10.1594/PANGAEA.741913>

- 875 [61] K. Mogensen, M. Balmaseda, A. Weaver, M. Martin, A. Vidard,
876 Nemovar: A variational data assimilation system for the nemo ocean
877 model, ECMWF newsletter 120 (2009) 17–22.
- 878 [62] K. Mogensen, M. A. Balmaseda, A. Weaver, et al., The nemovar ocean
879 data assimilation system as implemented in the ecmwf ocean analysis
880 for system 4 (2012).
- 881 [63] J. Waters, D. J. Lea, M. J. Martin, I. Mirouze, A. Weaver, J. While,
882 Implementing a variational data assimilation system in an operational
883 1/4 degree global ocean model, Quarterly Journal of the Royal Meteorological
884 Society 141 (687) (2015) 333–349.
- 885 [64] S. Kay, R. McEwan, D. Ford, North west european shelf production
886 centre northwestshelf_analysis_forecast_bio_004_011, quality information
887 document, Copernicus Marine Environment Monitoring Service (2019).
- 888 [65] R. R. King, J. While, M. J. Martin, D. J. Lea, B. Lemieux-Dudon, J. Waters,
889 E. O’Dea, Improving the initialisation of the met office operational
890 shelf-seas model, Ocean Modelling 130 (2018) 1–14.
- 891 [66] D. Ford, Assimilating synthetic biogeochemical-argo and ocean colour
892 observations into a global ocean model to inform observing system design,
893 Biogeosciences 18 (2) (2021) 509–534.
- 894 [67] S. Bloom, L. Takacs, A. Da Silva, D. Ledvina, Data assimilation using
895 incremental analysis updates, Monthly Weather Review 124 (6) (1996)
896 1256–1271.
- 897 [68] S. A. Good, M. J. Martin, N. A. Rayner, En4: Quality controlled
898 ocean temperature and salinity profiles and monthly objective analyses
899 with uncertainty estimates, Journal of Geophysical Research: Oceans
900 118 (12) (2013) 6704–6716.
- 901 [69] J. While, M. J. Martin, Variational bias correction of satellite sea-surface
902 temperature data incorporating observations of the bias, Quarterly Journal
903 of the Royal Meteorological Society 145 (723) (2019) 2733–2754.
- 904 [70] S. Sathyendranath, R. J. Brewin, C. Brockmann, V. Brotas, B. Calton,
905 A. Chuprin, P. Cipollini, A. B. Couto, J. Dingle, R. Doerffer, et al., An
906 ocean-colour time series for use in climate studies: The experience of the

- 907 ocean-colour climate change initiative (oc-cci), *Sensors* 19 (19) (2019)
908 4285.
- 909 [71] J. W. Campbell, The lognormal distribution as a model for bio-optical
910 variability in the sea, *Journal of Geophysical Research: Oceans* 100 (C7)
911 (1995) 13237–13254.
- 912 [72] A. D. Beaton, C. L. Cardwell, R. S. Thomas, V. J. Sieben, F.-E. Legiret,
913 E. M. Waugh, P. J. Statham, M. C. Mowlem, H. Morgan, Lab-on-chip
914 measurement of nitrate and nitrite for in situ analysis of natural waters,
915 *Environmental science & technology* 46 (17) (2012) 9548–9556.
- 916 [73] A. G. Vincent, R. W. Pascal, A. D. Beaton, J. Walk, J. E. Hopkins,
917 E. M. S. Woodward, M. Mowlem, M. C. Lohan, Nitrate drawdown dur-
918 ing a shelf sea spring bloom revealed using a novel microfluidic in situ
919 chemical sensor deployed within an autonomous underwater glider, *Ma-
920 rine Chemistry* 205 (2018) 29–36.
- 921 [74] A. Birchill, G. Clinton-Bailey, R. Hanz, E. Mawji, T. Cariou, C. White,
922 S. Ussher, P. Worsfold, E. P. Achterberg, M. Mowlem, Realistic measure-
923 ment uncertainties for marine macronutrient measurements conducted
924 using gas segmented flow and lab-on-chip techniques, *Talanta* 200 (2019)
925 228–235.
- 926 [75] I. Hinrichs, V. Gouretski, J. Päch, K. Emeis, D. Stammer, North sea
927 biogeochemical climatology (2017).
- 928 [76] E. O’dea, A. Arnold, K. Edwards, R. Furner, P. Hyder, M. Mar-
929 tin, J. Siddorn, D. Storkey, J. While, J. Holt, et al., An operational
930 ocean forecast system incorporating nemo and sst data assimilation for
931 the tidally driven european north-west shelf, *Journal of Operational
932 Oceanography* 5 (1) (2012) 3–17.
- 933 [77] M. E. Baird, P. G. Timko, L. Wu, The effect of packaging of chloro-
934 phyll within phytoplankton and light scattering in a coupled physical-
935 biological ocean model, *Marine and Freshwater Research* 58 (10) (2007)
936 966–981.
- 937 [78] S. G. Leles, L. Polimene, J. Bruggeman, J. Blackford, S. Ciavatta, A. Mi-
938 tra, K. J. Flynn, Modelling mixotrophic functional diversity and impli-

- 939 cations for ecosystem function, *Journal of Plankton Research* 40 (6)
940 (2018) 627–642.
- 941 [79] M. Goodliff, T. Bruening, F. Schwichtenberg, X. Li, A. Lindenthal,
942 I. Lorkowski, L. Nerger, Temperature assimilation into a coastal ocean-
943 biogeochemical model: assessment of weakly and strongly coupled data
944 assimilation, *Ocean Dynamics* 69 (10) (2019) 1217–1237.

Highlights:

- Biogeochemistry has a major influence over physics in the shelf seas.
- The modelled physics is sensitive to the representation of light.
- We tested a two-way coupled physical-biogeochemical model in the context of operational system.
- The two-way coupled model can moderately improve the timing of the phytoplankton bloom.

Jozef Skakala (Conceptualization, Formal analysis, Investigation, Methodology, Software, Validation, Visualisation, Writing - original draft, Writing - review & editing)

Jorn Bruggeman (Funding acquisition , Software, Supervision)

David Ford (Conceptualization, Software, Supervision, Roles/Writing - original draft; Writing - review & editing)

Sarah Wakelin (Software, Roles/Writing - review & editing)

Anil Akpinar (Data curation, Roles/Writing - original draft)

Tom Hull (Data curation, Roles/Writing - original draft)

Jan Kaiser (Data curation, Roles/Writing - original draft)

Benjamin R. Loveday (Data curation, Roles/Writing - original draft, Roles/Writing - review & editing)

Enda O'Dea (Supervision)

Charlotte Williams (Data curation, Roles/Writing - original draft)

Stefano Ciavatta (Funding acquisition, Project administration, Roles/Writing - original draft)

Declaration of interests

The authors declare that they have no known competing financial interests or personal relationships that could have appeared to influence the work reported in this paper.

The authors declare the following financial interests/personal relationships which may be considered as potential competing interests:

Journal Pre-proof